

Observational tests of the evolution of spheroidal galaxies and predictions for SIRTf/Spitzer cosmological surveys

L. Silva¹, G. De Zotti², G. L. Granato², R. Maiolino³, and L. Danese⁴

¹ INAF-Trieste, Via Tiepolo 11, I-34131 Trieste, Italy

² INAF-Padova, Vicolo Osservatorio 5, I-35122 Padova, Italy

³ INAF-Arcetri, Largo E. Fermi 5, I-50125 Firenze, Italy

⁴ SISSA, Via Beirut 4, I-34014 Trieste, Italy

Received / Accepted

Abstract. Granato et al. (2004) have elaborated a physically grounded model exploiting the mutual feedback between star-forming spheroidal galaxies and the active nuclei growing in their cores to overcome, in the framework of the hierarchical clustering scenario for galaxy formation, one of the main challenges facing such scenario, i.e. the fact that massive spheroidal galaxies appear to have formed much earlier and faster than predicted by previous hierarchical models, while the formation process was slower for less massive objects. Adopting the choice by Granato et al. (2004) for the parameters governing the history of the star formation, of chemical abundances and of the gas and dust content of galaxies, we are left with only two, rather constrained, but still adjustable, parameters, affecting the time- and mass-dependent SEDs of spheroidal galaxies. After having complemented the model with a simple phenomenological description of evolutionary properties of starburst, normal late-type galaxies, and of AGNs, we have successfully compared the model with a broad variety of observational data, including deep K -band, ISOCAM, ISOPHOT, IRAS, SCUBA, radio counts, and the corresponding redshift distributions, as well as the 1–1000 μm background spectrum. Special predictions have been made for the especially challenging counts and redshift distributions of EROs. We also present detailed predictions for the GOODS and SWIRE surveys with the Spitzer Space Telescope. We find that the GOODS deep survey at 24 μm and the SWIRE surveys at 70 and 160 μm are likely to be severely confusion limited. The GOODS surveys in the IRAC channels (3.6 to 8 μm), reaching flux limits of a few mJy, are expected to resolve most of the background at these wavelengths, to explore the full passive evolution phase of spheroidal galaxies and most of their active star-forming phase, detecting galaxies up to $z \approx 4$ and beyond. A substantial number of high z star-forming spheroidal galaxies should also be detected by the 24 μm SWIRE and GOODS surveys, while the 70 and 160 μm will be particularly useful to study the evolution of such galaxies in the range $1 \lesssim z \lesssim 2$. However, starburst galaxies at $z \lesssim 1$ –1.5 are expected to be the dominant population in MIPS channels, except, perhaps, at 160 μm .

Key words. galaxies: elliptical and lenticular, cD — galaxies: evolution — galaxies: formation — QSOs: formation

1. Introduction

The standard Lambda Cold Dark Matter (ΛCDM) cosmology is a well established framework to understand the hierarchical assembly of dark matter (DM) halos. Indeed, it has been remarkably successful in matching the observed large-scale structure. However the complex evolution of the baryonic matter within the potential wells determined by DM halos is still an open issue, both on theoretical and on observational grounds.

Full simulations of galaxy formation in a cosmological setting are far beyond present day computational possibilities. Thus, it is necessary to introduce at some level rough parametric prescriptions to deal with the physics of baryons, based on sometimes debatable assumptions (e.g. Binney 2004). A class of such models, known as semi-analytic models, has been extensively compared with the available information on

galaxy populations at various redshifts (e.g. Lacey et al. 1993; Kauffmann, White & Guiderdoni, 1993; Cole et al. 1994; Kauffmann et al. 1999; Somerville & Primack 1999; Cole et al. 2000; Granato et al. 2000; Benson et al. 2003).

The general strategy consists in using a subset of observations to calibrate the many model parameters providing a heuristic description of baryonic processes we don't properly understand. Besides encouraging successes, current semi-analytic models have met critical inconsistencies which seems to be deeply linked to the standard recipes and assumptions. These problems are in general related to the properties of elliptical galaxies, such as the color-magnitude and the $[\alpha/\text{Fe}]$ - M relations (Cole et al. 2000; Thomas 1999; Thomas et al. 2002), and the statistics of sub-mm and deep IR selected (I- and K-band) samples (Silva 1999; Chapman et al. 2003; Kaviani et al. 2003; Daddi et al. 2004; Kashikawa et al. 2003; Poli et al.

2003; Pozzetti et al. 2003; Somerville et al. 2004; see Cimatti 2003 for a review).

However, the general agreement of a broad variety of observational data with the hierarchical scenario and the fact that the observed number of luminous high-redshift galaxies, while substantially higher than predicted by semi-analytic models, is nevertheless consistent with the number of sufficiently massive dark matter halos, indicates that we may not need alternative scenarios, but just some new ingredients.

Previous work by our group (Granato et al. 2001; Romano et al. 2002; Granato et al. 2004) suggests that a crucial ingredient is the mutual feedback between spheroidal galaxies and active nuclei at their centers.

Granato et al. (2004, henceforth GDS04) presented a detailed physically motivated model for the early co-evolution of the two components, in the framework of the Λ CDM cosmology.

In this paper, we present a comprehensive comparison of the model with the available data (number counts and redshift distributions) in near-IR (NIR) to sub-mm bands and extensive predictions relevant for surveys such as GOODS and SWIRE, which are being carried out with NASA Spitzer (formerly SIRTf) Observatory. In Sect. 2 we give a short overview of the GDS04 model for spheroidal galaxies, a description of the phenomenological approach adopted to model the evolution of starburst and normal late-type galaxies, and of active galactic nuclei (AGNs). In Sect. 3 we discuss the determination of the two main parameters controlling the time-dependent spectral energy distributions (SEDs) of spheroidal galaxies. In Sect. 4, the model counts and redshift distributions are compared with data from the ISO surveys and follow-up, from the IRAS $60\mu\text{m}$ survey, from the SCUBA $850\mu\text{m}$ surveys and follow-up, from the radio 1.4 GHz surveys down to sub-mJy flux densities, and from deep K-band surveys and follow-up. In Sect. 5, we present our predictions for Spitzer GOODS and SWIRE surveys. The main conclusions are summarized in Sect. 6.

We adopt the following cosmological parameters: $\Omega_m = 0.3$, $\Omega_\Lambda = 0.7$, $H_0 = 70 \text{ km s}^{-1}$.

2. Model description

2.1. The GDS04 model

The model follows with simple, physically grounded, recipes and a semi-analytic technique the evolution of the baryonic component of proto-spheroidal galaxies within massive dark matter (DM) halos forming at the rate predicted by the standard hierarchical clustering scenario for a Λ CDM cosmology. The main difference with other treatments is in the central role attributed to the mutual feedback between star formation and growth of a super massive black hole (SMBH) in the galaxy center.

The kinetic energy fed by supernovae is increasingly effective, with decreasing halo mass, in slowing down (and eventually halting) both the star formation and the gas accretion onto the central black hole. On the contrary, star formation and black hole growth proceed very effectively in the more massive halos, until the energy injected by the active nucleus in the surround-

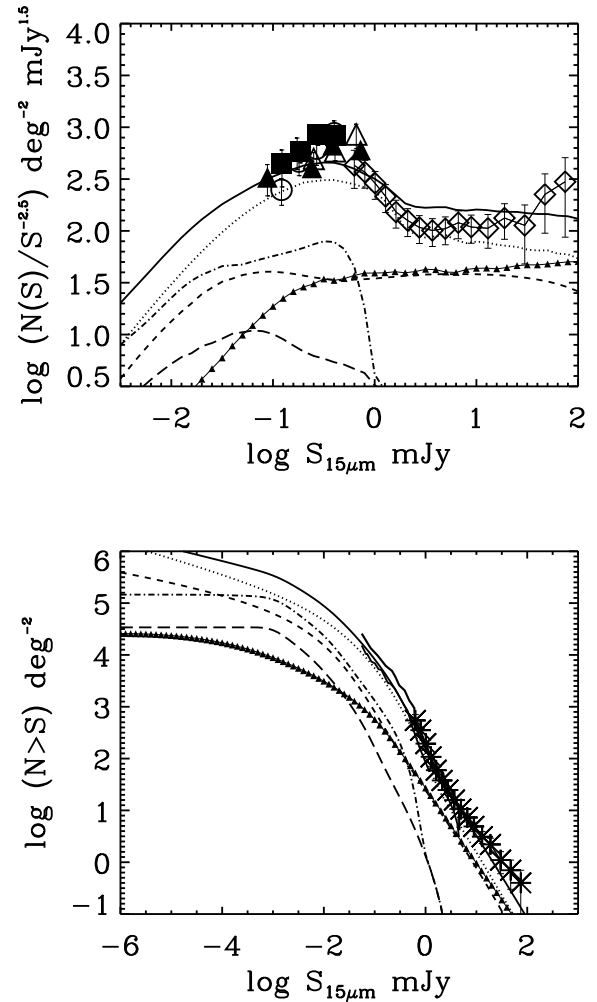


Fig. 1. Differential (upper panel) and integral (lower panel) $15\mu\text{m}$ counts. The solid line is the sum of contributions from spheroids (dot-dashed line; long dashes single out passively evolving spheroids), spirals (short dashes), starburst galaxies (dotted line) and (type 1 + 2) AGN (filled triangles). Data are from Elbaz et al. (1999), Gruppioni et al. (2002).

ing interstellar gas unbinds it, thus halting both the star formation and the black hole growth (and establishing the observed relationship between black hole mass and stellar velocity dispersion or halo mass). As a result, the physical processes acting on baryons reverse the order of the formation of spheroidal galaxies with respect to the hierarchical assembling of DM halos, in keeping with the previous proposition by Granato et al. (2001).

Not only the black hole growth is faster in more massive halos, but also the feedback of the active nucleus on the interstellar medium is stronger, to the effect of sweeping out such medium earlier, thus causing a shorter duration of the active star-formation phase (for more details, see GDS04).

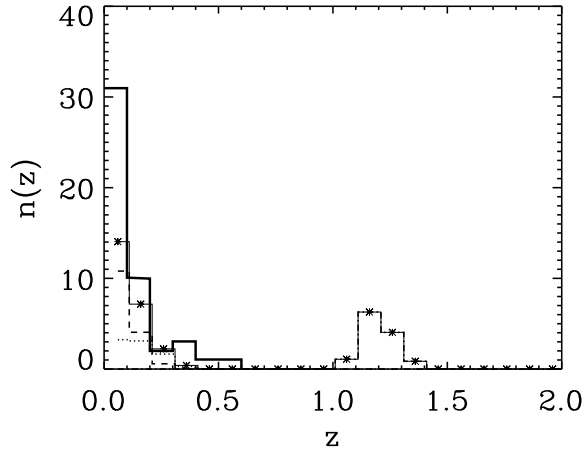
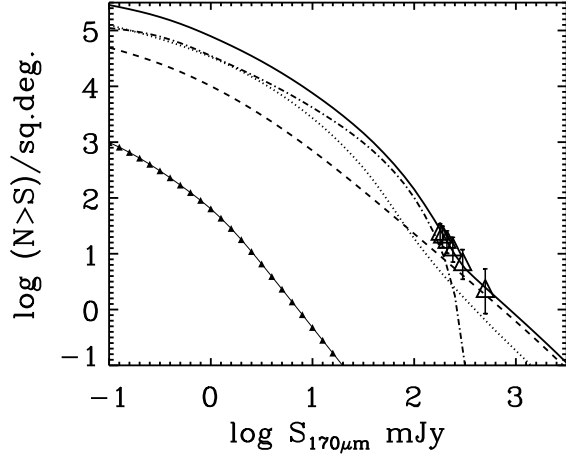


Fig. 2. $170\mu\text{m}$ counts (upper panel) and redshift distribution of sources with $S_{170} > 223\text{ mJy}$ over an area of 3 deg^{-2} . The dotted, dashed, dot-dashed lines and the filled triangles show the contributions of starburst, spiral, (star-forming) spheroidal galaxies and AGN, respectively. Data in the upper panel are by Dole et al. (2001). In the lower panel, the thin continuous line with asterisks is the sum of the various contributions and the thick continuous histogram shows the data by Rowan-Robinson et al. (2003).

2.2. Spectral energy distribution of spheroidal galaxies

As in GDS04, we compute the SEDs of spheroidal galaxies using our code GRASIL, described in Silva et al. (1998; for subsequent improvements and updates see <http://web.pd.astro.it/granato>). GRASIL computes the time-dependent UV to radio SED of galaxies, given their star formation and chemical enrichment histories (derived as described in the previous section), and with a state of the art treatment of dust reprocessing. The latter point is fundamental, since during the phase of intense star-formation, young stars are mixed with a huge amount of gas, quickly chemically enriched and dust polluted. The use of local templates (such as M82 or Arp220) may be inappropriate in these extreme conditions. Broadly

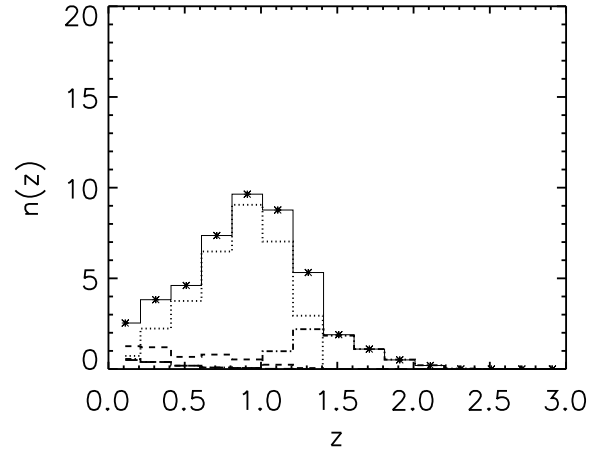
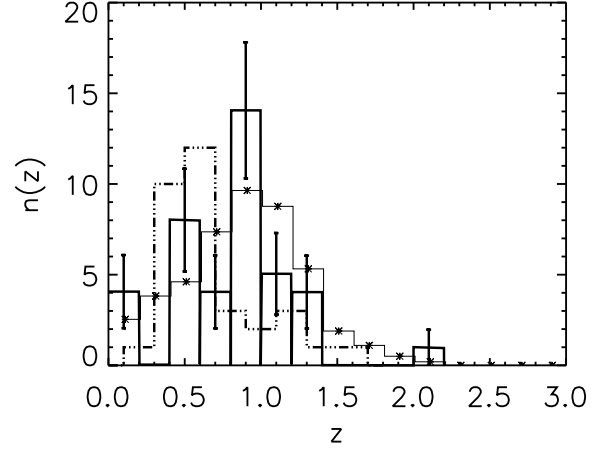


Fig. 3. Redshift distribution of sources brighter than 0.1 mJy at $15\mu\text{m}$, within an area of $6 \cdot 10^{-3}\text{ deg}^2$. In the upper panel the global (spheroids plus spiral and starburst galaxies) redshift distribution predicted by the model (thin continuous line with asterisks) is compared with data by Elbaz et al. (2002, thick solid histogram with error bars) and by Franceschini et al. (2003, three dot-dashed line). In the lower panel we show the various contributions to the global model distribution (again shown by the thin solid histogram with asterisks): starbursts (dots), spirals (dashes), star-forming spheroids (dots-dashes), passively evolving spheroids (long dashes).

speaking, predictions of fluxes during the active star forming phase become more and more affected by model uncertainties at shorter and shorter wavelengths.

One of the most important distinctive features of GRASIL is that it has included, for the first time, the effect of *differential extinction* of stellar populations (younger stellar generations are more affected by dust obscuration), due to the fact that stars form in a denser than average environment, the molecular clouds, and progressively get rid of them.

While in principle the GRASIL SEDs depend on several parameters, in the conditions envisaged here only two of them

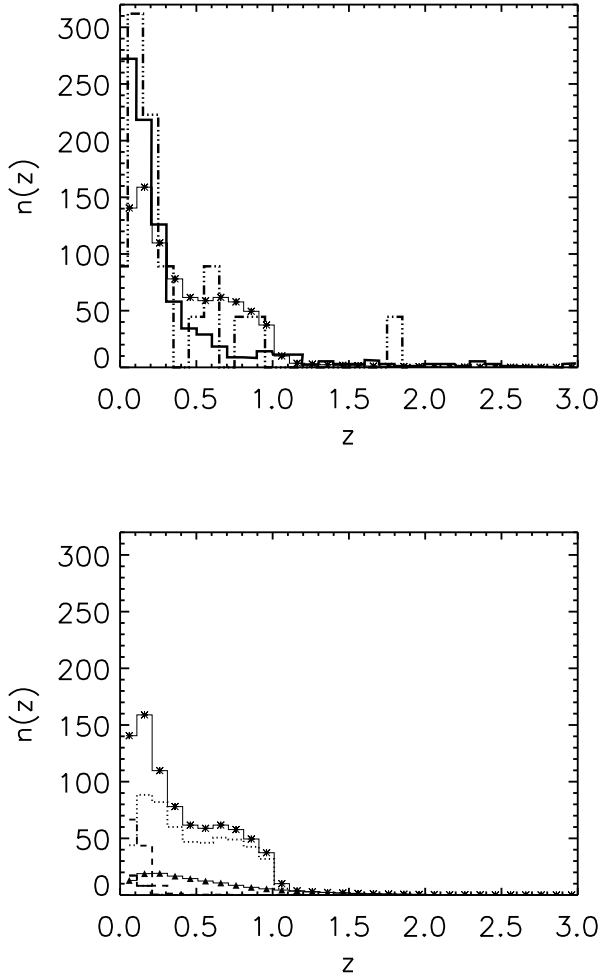


Fig. 4. Redshift distribution of sources brighter than 1 mJy at $15\mu\text{m}$, within an area of 5.46 deg^{-2} . In the upper panel the global (spheroids plus spirals, starbursts and AGN) model z -distribution (thin continuous line with asterisks) is compared with data by Rowan-Robinson et al. (2003, thick continuous line) and Pozzi et al (2003; three dots-dash, scaled to the same area). In the lower panel, the dotted, short-dashed, dot-dashed lines and the filled triangles show the contributions from starburst, spiral, spheroidal galaxies, and AGN respectively, to the global redshift distribution, represented again by the thin continuous line with asterisks. The long-dashed line singles out the contribution of passively evolving spheroids.

are really important: the dust optical depth of molecular clouds (τ_{MC}), and the escape time scale (t_e) of young stars from their parent molecular clouds. The latter affects more directly the predictions for the optical-NIR regions and has been determined fitting the K-band data. The former affects the entire SED, and is proportional to the dust to gas mass ratio δ and to $M_{\text{MC}}/r_{\text{MC}}^2$, M_{MC} and r_{MC} being the typical mass and radius of molecular clouds, respectively. We have simply assumed that δ increases linearly with the gas metallicity (e.g., Dwek 1998) and is $\approx 1/100$ (the Galactic value) for solar metallicity. The ra-

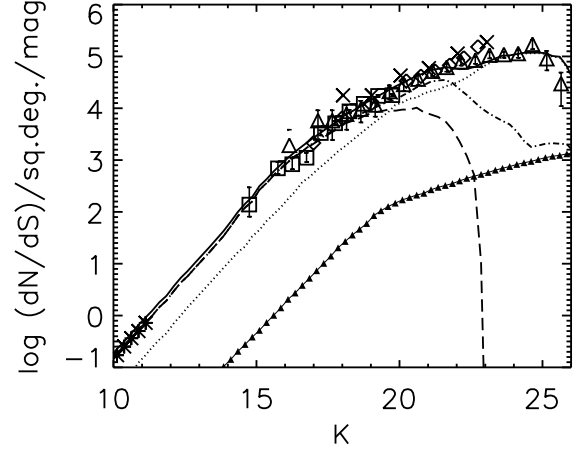


Fig. 5. K-band counts. Dot-dash: spheroids (the long-dashed line singles out passively evolving spheroids); dots: late type galaxies (spirals, irregulars and dwarves), assumed not to evolve in the near-IR band (see text); filled triangles: AGN. We have assumed $t_e = 0.05$ Gyr for star-forming spheroids (see text); with this choice, they show up at $K \gtrsim 19$ and become increasingly important with increasing K up to $K \approx 22$. Data from Moustakas et al. (1997), Kochanek et al. (2001), Saracco et al. (2001), Totani et al. (2001), Cimatti et al. (2002).

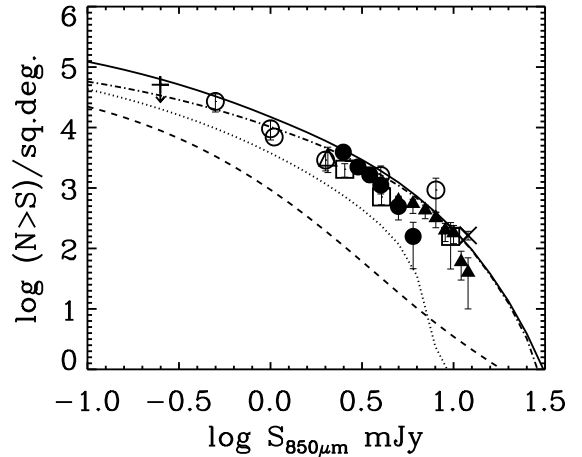


Fig. 6. $850\mu\text{m}$ counts. The dot-dashed, dotted, and dashed lines refer to (star-forming) spheroids, starburst, and spiral galaxies, respectively, while the solid line is the sum of the various contributions. AGN are not visible within the limits of the plot. Data from Blain et al. (1999), Hughes et al. (1998), Barger, Cowie, & Sanders (1999), Eales et al. (2000), Chapman et al. (2002), Borys et al. (2002).

tio $M_{\text{MC}}/r_{\text{MC}}^2$ has been allowed to vary within a range of values compatible with those found for typical giant molecular clouds in the Milky Way ($M_{\text{MC}} \sim 10^6 M_{\odot}$, $r_{\text{MC}} \sim 15$ pc).

As for t_e , it actually represents the time during which stars are within an environment of high optical depth (τ_{MC}) since

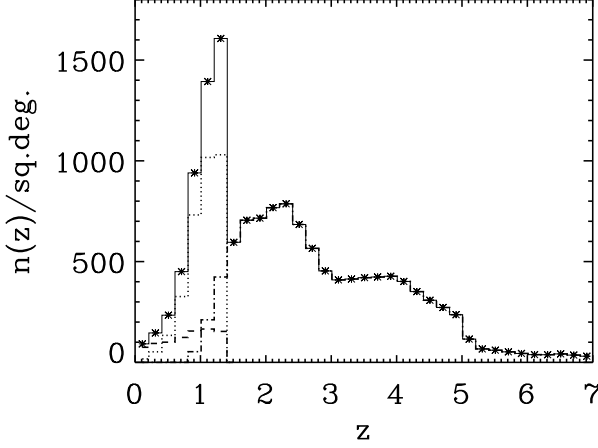


Fig. 7. Redshift distributions of sources brighter than 1 mJy at $850\mu\text{m}$. The dot-dashed, dotted, and dashed lines refer to (star-forming) spheroids, starburst, and spiral galaxies, respectively, while the thin solid line with asterisks is the sum of the various contributions.

GRASIL assumes a small optical depth (due to cirrus) outside molecular clouds. This is likely to be unrealistic in the extreme conditions envisaged here during the fast star forming phase of spheroids, particularly in the dense central regions. Indeed in this case there is a high probability that a light ray coming from a star outside its parent molecular cloud intersects at least one molecular cloud over a typical galactic path. Our cure for this problem is described in Sect. 3.

2.3. Prescriptions for other galaxy populations

We use the GDS04 prescriptions to model the star formation occurring within DM halos (up to a maximum mass of $\log(M_{\text{vir,max}}/M_{\odot}) = 13.2$) virialized at $z_{\text{vir}} \gtrsim 1.5$ and $M_{\text{vir}} \gtrsim 10^{11.6} M_{\odot}$. The latter cuts are meant to crudely filter out galactic halos associated with a spheroidal galaxy. We envisage disks (and irregulars) as associated primarily to halos virializing at $z_{\text{vir}} \lesssim 1.5$, which have incorporated, through merging processes, a large fraction of halos less massive than $4 \times 10^{11} M_{\odot}$ virializing at earlier times. The latter may become the bulges of late type galaxies. However, we do not address here the physics of the formation of disk (and irregular) galaxies. Their contributions to number counts are estimated following, as usual, a phenomenological approach, which consists in simple analytic recipes to evolve their local luminosity functions (LFs), and appropriate templates for their SEDs to compute K-corrections and to extrapolate the models to different wavelengths where direct determinations of the local luminosity functions are not available.

We adopt the simplest assumptions that are able to describe the counts and redshift distributions of these populations. The prescriptions applying in the mid-IR (MIR) to sub-mm spectral region are different from those in the optical/near-IR (NIR), due to the different emission mechanisms. Indeed it is well

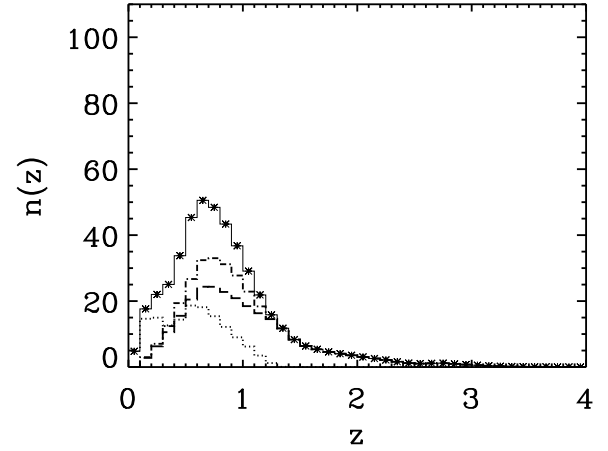
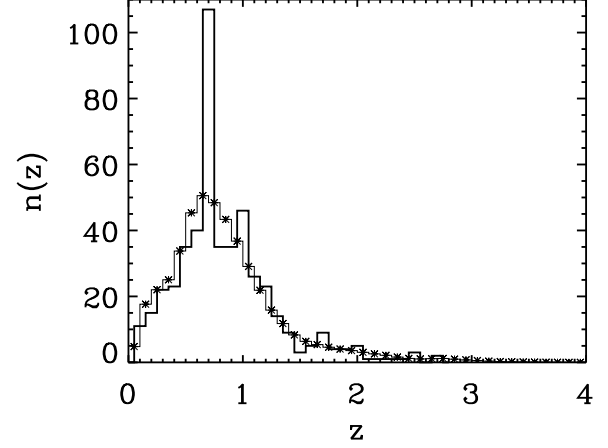


Fig. 8. Redshift distribution of galaxies brighter than $K = 20$. In the upper panel the total model distribution (thin line with asterisks) is compared with the, mostly spectroscopic, data by Cimatti et al. (2002; thick solid line). The lower panel details the various contributions (dots: non-evolving late type galaxies; dot-dash: spheroids). The long-dashed line singles out passively evolving spheroids.

known that galaxies with very different far-IR (FIR) SEDs can have similar optical-NIR SEDs. This is clearly witnessed also by the comparison between the FIR luminosity functions (e.g. Saunders et al. 1990) and the optical ones. Only the latter is well described by the Schechter parameterization.

2.3.1. Mid-IR to sub-mm region

The IRAS and ISO survey data can be interpreted (e.g., Franceschini et al. 2001; Gruppioni et al. 2002) in terms of a slowly evolving population of spiral (and irregular) galaxies (SPs), and a rapidly evolving population of starburst galaxies (SBs). We adopt the $60\mu\text{m}$ local LFs by Saunders et al (1990), that have been derived for “warm” and “cold” galaxies (based

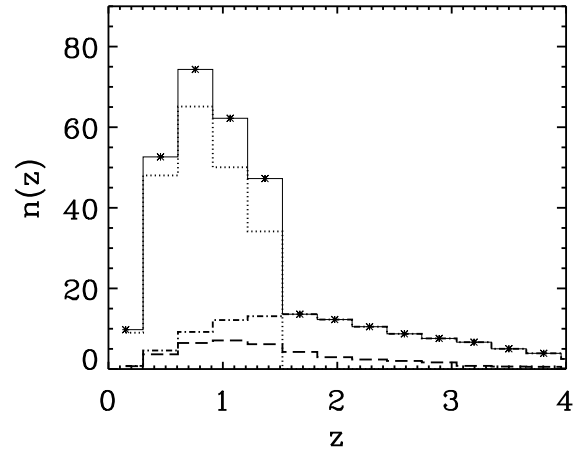
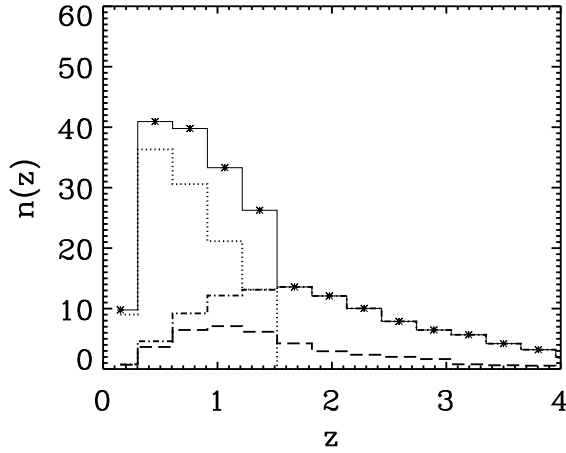
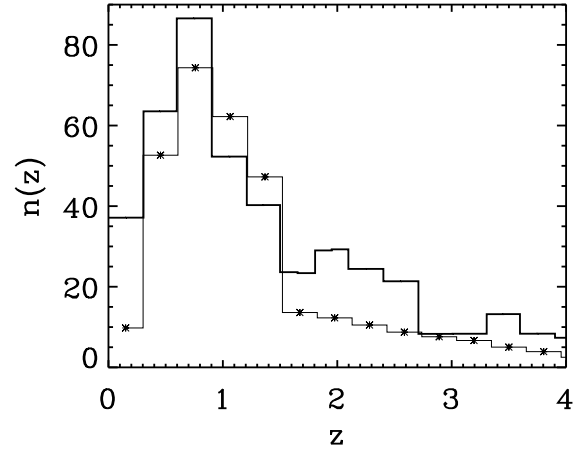
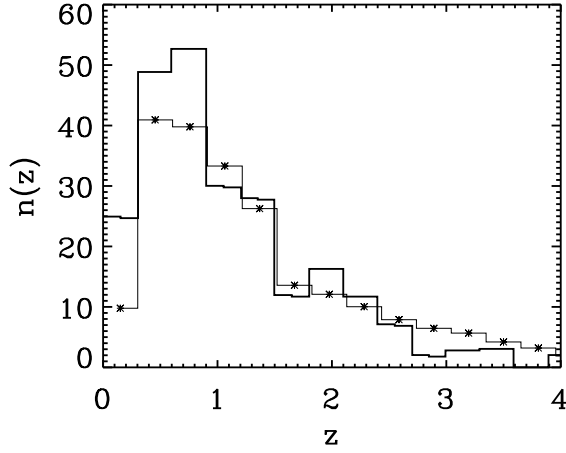


Fig. 9. Redshift distribution of galaxies brighter than $K = 23$. The meaning of the lines is the same as in Fig. 8. Data (photometric redshifts) from the Subaru deep survey (Kashikawa et al. 2003).

Fig. 10. Redshift distribution of galaxies brighter than $K = 24$. The meaning of the lines is the same as in Fig. 8. Data (photometric redshifts) from the Subaru deep survey (Kashikawa et al. 2003).

on IRAS colors) that we associate, respectively, to SBs and SPs.

For SBs we used, as templates, the SEDs of NGC6090 and of M82 (Silva et al. 1998). However, both these galaxies have 15 to 60 μm luminosity ratios, $L_{15}/L_{60} \simeq 0.08$, somewhat higher than the average value for active star forming galaxies selected at 60 μm ($< L_{15}/L_{60} > \simeq 0.05$; Mazzei et al. 2001) and for nearby bright galaxies ($< L_{15}/L_{60} > \simeq 0.04$; Dale et al. 2000). We take $L_{15}/L_{60} = 0.05$ to extrapolate to 15 μm the 60 μm SB local LF.

Unless otherwise noted, we have adopted the SED of NGC6090, which turns out to be closer to the SEDs of starburst galaxies detected by the ISO FIRBACK survey (Chapman et al. 2002; Sajina et al. 2003; Patris et al. 2003). This is clearly a quite crude approximation since the starburst SEDs are known to vary systematically with luminosity (Xu et al. 2001; Chapman et al. 2003; Lagache et al. 2003). A more detailed treatment of the starburst SEDs is however beyond the

scope of the present paper, which is focussed on spheroidal galaxies. We have therefore chosen to adopt, for the other populations, the simplest models still compatible with the data.

The evolutionary parameters of SBs were determined from fits of the 15 μm counts and redshift distributions. Consistent with earlier analyses, we find that both density and luminosity evolution is required for the SB population, with $LF[L(z), z] = LF[L(z)/(1+z)^{2.5}, z=0] \times (1+z)^{3.5}$. Not to exceed the bright 15 μm source counts we had to cut off the local LF at $L_{60\mu\text{m}} = 2 \times 10^{32}$ erg/s/Hz. A similar high-luminosity cut-off was introduced by Gruppioni et al. (2002) and Pozzi et al. (2003).

As for SPs, we use a pure luminosity evolution model, $L(z) = L(0)(1+z)^{1.5}$ and the SED of the Sc galaxy NGC6946. Again, a detailed analysis of the contributions of SPs to the counts and to the redshift distributions at the various wavelengths, allowing for their colour distribution as well as for the

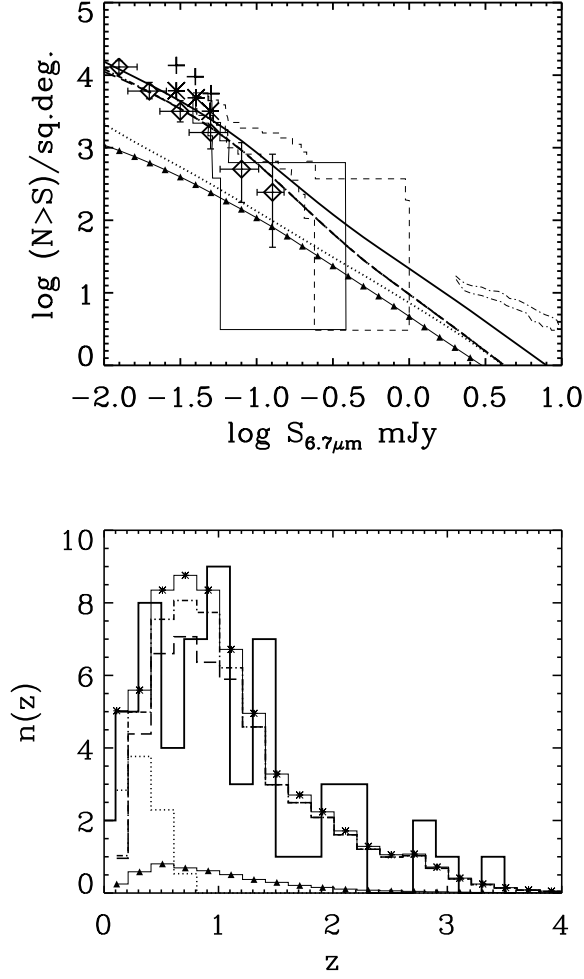


Fig. 11. $6.7\mu\text{m}$ counts and redshift distribution of sources with $S_{6.7} > 10\mu\text{Jy}$ within 16 arcmin^2 . The dot-dashed and dotted lines refer to spheroids (mostly passively evolving, as illustrated by the long dashed line, detailing their contribution to the redshift distribution in the lower panel) and to non-evolving late-type galaxies, respectively. The filled triangles refer to AGN. Their total is the thin line with asterisks. The thick continuous line in the redshift distribution is from Sato et al. (2004). Observed counts from Taniguchi et al. (1997), Altieri et al. (1999), Serjeant et al. (2000), Oliver et al. (1997, 2002), Sato et al. (2003).

cold galaxies discovered by the ISOPHOT serendipity survey (Stickel et al. 2000), is beyond the scope of the present paper.

The LFs of both SBs and SPs are assumed to evolve as described above up to $z = 1$ and to keep constant afterwards, up to a redshift cut-off $z_{\text{cutoff}} = 1.5$, above which essentially all the massive halos are associated, according to GDS04, with spheroidal galaxies.

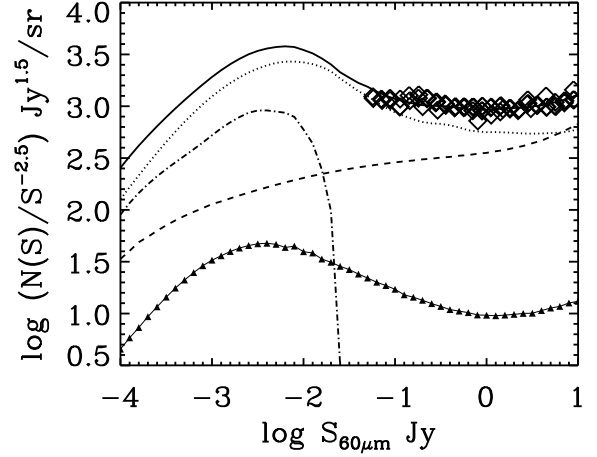


Fig. 12. IRAS $60\mu\text{m}$ differential counts. Dotted line: starbursts; dashed line: spirals; dot-dashed line: (star-forming) spheroids; filled triangles: AGN; solid line: total. Data from Mazzei et al. (2001), Lonsdale et al. (1990), Pearson & Rowan-Robinson (1996), Bertin et al. (1997).

2.3.2. Near-IR region

The rest-frame NIR SED is generally dominated by old and slowly evolving low mass stars. To estimate the contribution of all late-type galaxies (including starburst galaxies) to the counts, the redshift distributions and the background intensity in the range $1\text{--}10\mu\text{m}$, we have adopted the R-band local LF for intermediate and late-type galaxies by de Lapparent et al. (2003), and the SED of NGC6946. The LF is assumed not to evolve and, again, a redshift cut-off $z_{\text{cutoff}} = 1.5$ is introduced.

2.4. Active Galactic Nuclei

We have also included the contribution of the nuclear emission by AGNs (type 1 and 2) to the source counts, computed as in Silva, Maiolino, & Granato (2004): the cosmological evolution of AGNs, derived from X-ray surveys (Ueda et al. 2003), has been coupled to an accurate definition of the average X-ray to sub-mm SEDs of AGNs, as a function of the absorption column densities N_H .

3. Determination of the GRASIL parameters for spheroidal galaxies

As already mentioned, we need to determine two GRASIL parameters: the dust optical depth of molecular clouds (τ_{MC}), and the escape time scale (t_e) of young stars from their parent molecular clouds. The former quantity determines, in particular, the contribution (if any) of star-forming spheroidal galaxies to the bump in the $15\mu\text{m}$ counts below a few mJy. Although the observed counts are affected by a considerable uncertainty, as shown by the spread of results from different surveys, and the modelling is complicated by the presence of PAH bands, they can be interpreted in terms of evolving SBs, with a minor contribution to SPs, particularly at the brighter flux den-

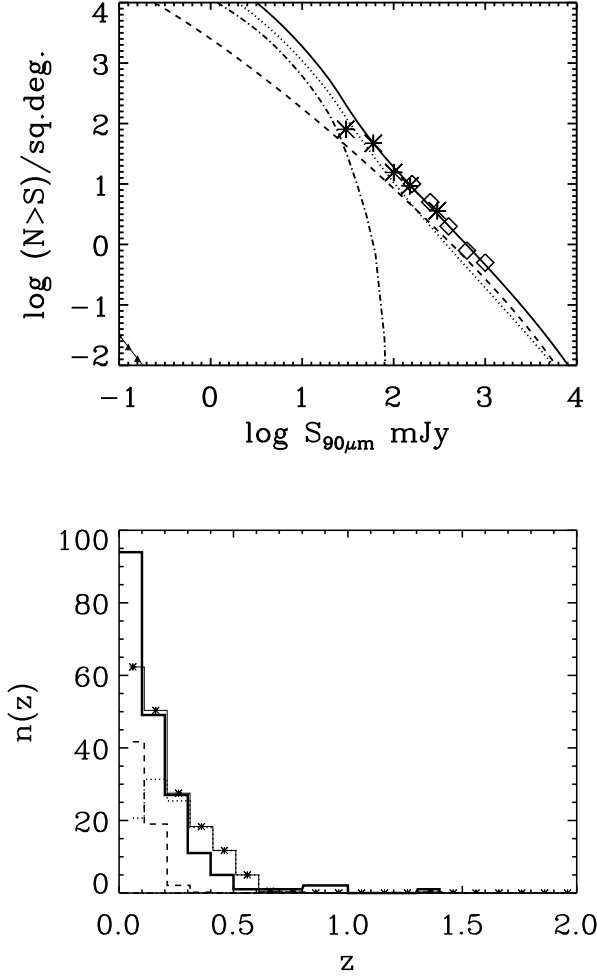


Fig. 13. $90\mu\text{m}$ counts and redshift distribution of sources with $S_{90} > 70 \text{ mJy}$ within 5.34 deg^{-2} . The SB SED is that of NGC6090. Dotted line: starbursts; dashed line: spirals; dot-dashed line: spheroids; filled triangles: AGN. The solid line in the upper panel and the thin continuous histogram with asterisks in the lower panel show the sum of all contributions. The thick continuous histogram displays the observed z -distribution by Rowan-Robinson et al. (2003). Observed counts from Efstathiou et al. (2000) and Rodighiero et al. (2003).

sity levels. Thus, the observed $15\mu\text{m}$ flux from star-forming spheroids must be substantially suppressed, implying $\tau_{\text{MC}} \gtrsim 40$ at $1\mu\text{m}$ (see Fig. 1). On the other hand, a too large value of τ_{MC} would entail a too large contribution from such sources to the $170\mu\text{m}$ counts (see Fig. 2). In the following we set $\tau_{\text{MC}} \approx 45$ at $1\mu\text{m}$, a value yielding a small, but non-negligible, contribution to the sub-mJy $15\mu\text{m}$ counts and a significant contribution to the $170\mu\text{m}$ counts below a few hundred mJy, somewhat improving the quality of the fit in both cases (Figs. 1 and 2).

The redshift distribution for $S_{15\mu\text{m}} \geq 0.1 \text{ mJy}$ (Aussel et al. 1999; Elbaz et al. 2002; Franceschini et al. 2003) is also satisfactorily reproduced (Fig. 3) and that for $S_{15\mu\text{m}} \geq 1 \text{ mJy}$ is

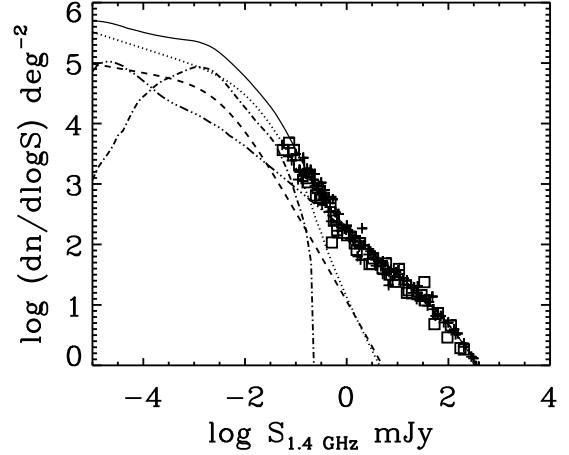


Fig. 14. 1.4 GHz counts. Dotted line: starbursts; dashed line: spirals; dot-dashed line: spheroids; three dots-dash line: sum of flat- and steep-spectrum radio galaxies according to models by Dunlop & Peacock (1990). Data from Windhorst et al. (1993), Gruppioni et al. (1997, 1999), Ciliegi et al. (1999), Hopkins et al. (1999), Richards (2000).

also consistent with the limited information currently available (Fig. 4; Pozzi et al. 2003; Rowan-Robinson et al. 2003).

Sajina et al. (2003) derived photometric redshifts for a representative sample of 30 sources detected in the FIRBACK $170\mu\text{m}$ survey to a limiting flux density of $S_{170\mu\text{m}} \geq 135 \text{ mJy}$. The estimated redshift distribution turns out to be bimodal, most sources being at $z \ll 1$, but with a clump of 5 sources at $z \sim 0.4$ – 1 . The redshift distribution predicted by our model has roughly the correct ratio of low to high redshift sources, but the mean redshift of the latter is somewhat higher than estimated by Sajina et al. (2003). The redshift measurements, 90% complete, of brighter ($S_{170\mu\text{m}} \geq 200 \text{ mJy}$; 4σ detections) FIRBACK sources by Patris et al. (2003) have shown that the vast majority of them are moderate luminosity dusty galaxies at $z < 0.3$, with a rather cold SED. In Fig. 2 the redshift distribution yielded by our model for $S \geq 223 \text{ mJy}$ is compared with data by Rowan-Robinson et al. (2003). As discussed below, the predicted peak at $z > 1$ due to star-forming galaxies, not seen in the data, may be due to our rough treatment of their optically thick phase. A slight decrease of the 170 to $850\mu\text{m}$ flux density ratio compared to that yielded by GRASIL or a slightly lower value of τ_{MC} is enough to get rid of the $z > 1$ peak.

The parameter t_e is meant (cf. Sect. 2.2) to control the fraction of star-light, produced in star-forming spheroidal galaxies, which is only reprocessed by cirrus dust, and is therefore observable at optical wavelengths.

Since GRASIL assumes that the gas (and the dust) is in molecular clouds (MCs) and in the cirrus, the mean optical depth to a star outside its parent MC, τ_{outside} , is equal to $\tau_{\text{cirrus}} + \bar{N} \times 2\tau_{\text{MC}}$, \bar{N} being the mean number of MCs along its line of sight, which is roughly proportional to the size of the galaxy (or, for given virialization redshift, to $M_{\text{vir}}^{1/3}$). Thus, for small enough galaxies the optical depth drops from τ_{MC} to

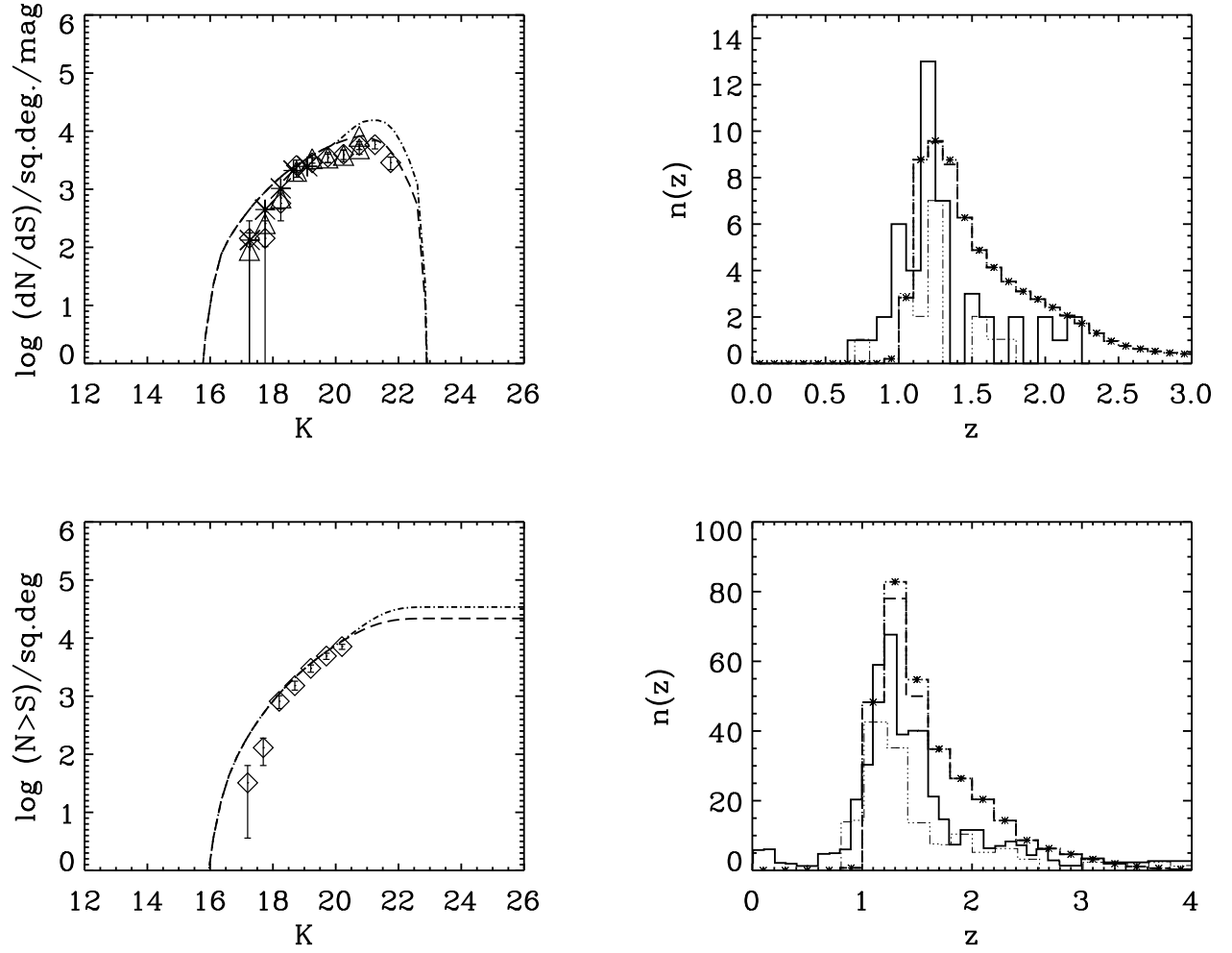


Fig. 15. Differential and integral K-band counts for EROs ($R - K > 5$). The long dashed and dot-dashed lines show the predicted counts of passively evolving spheroids and of all spheroids (including the star-forming ones). Data in the upper panel are from Roche et al. (2002, 2003), and Daddi et al. (2000). In the lower panel model predictions are compared with the counts of old (passively evolving) EROs by Miyazaki et al. (2003).

τ_{cirrus} , which is $\ll 1$ at IR wavelengths, when the stars move out of their parent MCs, after a time t_e . This same condition is met in most cases when dealing with relatively normal galaxies, even moderate starbursts (e.g. when reproducing the SED of nearby galaxies), where the covering factor of MCs is $\ll 1$. On the contrary, for large galaxies and for the really extreme conditions met in forming spheroids according to our scenario, τ_{outside} can be substantially larger than τ_{MC} . The present release of GRASIL, however, does not allow us to deal accurately with the radiation transfer through the distribution of MCs. On the other hand, such detailed treatment is not crucial for our present purposes since whenever $\tau_{\text{outside}} \geq \tau_{\text{MC}}$ essentially all the starlight is reprocessed by dust. We have crudely approximated τ_{outside} as a step function: $\tau_{\text{outside}} = \tau_{\text{cirrus}}$

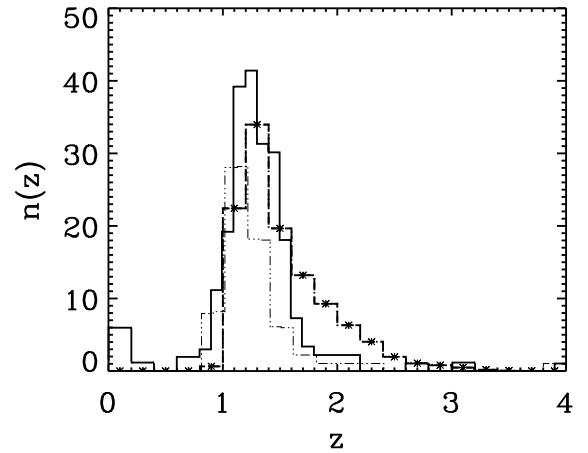


Fig. 16. From top to bottom: redshift distribution of EROs with $K < 20$ in the K20/CDFS survey area (32.2 arcmin², Cimatti et al. 2003), $K < 20.3$ and $K < 19.2$ (114 arcmin², Miyazaki et al. 2003). The observed redshift distributions including both passively evolving and star-forming EROs are shown by the thick solid lines, while the three dots-dashed lines refer to the passively evolving only. The model distributions are represented by the dot-dashed lines with asterisks (all EROs) and by the long-dashed lines (passively evolving only).

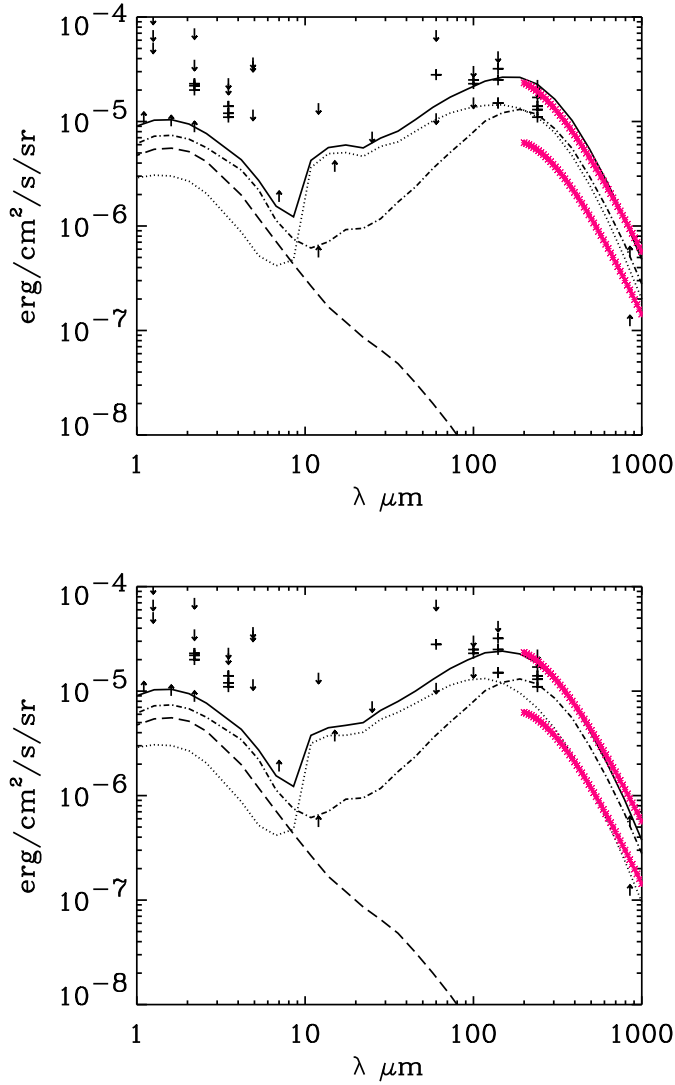


Fig. 17. Contributions to the 1 – 1000 μ m background from spheroids (dot-dash; passively evolving spheroids are represented by long dashes) and late-type galaxies (dots). The leap of the dotted line at 10 μ m corresponds to the transition between the two evolutionary regimes for late type galaxies (see text). The thick solid line shows the sum of all contributions. In the upper panel we have used the SED of NGC6090 for starburst galaxies, while in the lower one we have used that of M82. The SED parameters for forming spheroids are those described in Sect. 3, i.e. $\tau_{MC,1\mu m} = 45$, and $t_e = 0.05$ Gyr for low mass spheroids, t_e equal to the starburst duration for the massive ones. Data are from Hauser & Dwek (2001).

for $M_{vir} \leq M_{vir,crit}$ and $\tau_{outside} = \tau_{cirrus} + \tau_{MC}$ for larger virial masses. In order to take into account the dust heating by the absorbed starlight, in practice we have kept the stars within their MCs for the full duration of the starburst, for galaxies with $M_{vir} \geq M_{vir,crit}$.

This treatment may overestimate the duration of the optically thick phase, as well as the optical thickness, of the relatively less massive galaxies (but still with $M_{vir} \geq M_{vir,crit}$)

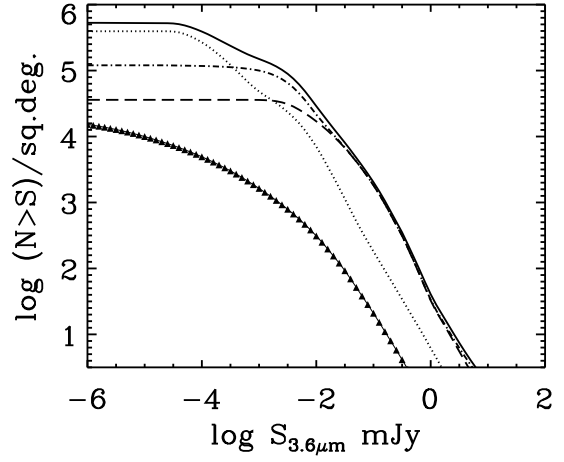


Fig. 18. Predicted 3.6 μ m IRAC source counts. Dot-dashed line: spheroids (the contribution of passively evolving spheroids is shown by the long-dashed line); dotted line: late type galaxies; filled triangles: AGNs. The total counts are shown by the solid line.

which are responsible for the peak at $z > 1$ in the redshift distribution at 170 μ m, predicted by the model but not seen (Fig. 2). We thus expect that, with a more realistic treatment, we will get rid of such peak.

We find that, for the value of τ_{MC} derived as explained above, we can account for the K-band counts assuming for t_e a value between ≈ 0.05 and 0.4 Gyr and setting $M_{vir,crit} \approx 10^{12} M_{\odot}$. The results in Fig. 5 refer to $t_e = 0.05$ Gyr and illustrate the relative contributions of star-forming and passively evolving spheroids, as well as of starburst and spiral galaxies.

4. Comparison with the data

4.1. Counts and redshift distributions

As discussed by Granato et al. (2001, 2004), in the present framework the SCUBA-selected galaxies are interpreted as being mostly star-forming spheroids ($M_{vir} \geq 10^{11.6} M_{\odot}$). This is borne out by Figs. 6 and 7. The values of GRASIL parameters derived above yield a good fit to the 850 μ m SCUBA counts, while significantly higher/lower values of the optical depth of star-forming spheroidal galaxies would lead to a substantial over/under-prediction of the counts. The contributions of other populations, such as normal late-type galaxies, radio sources, and starburst galaxies are only important at flux density levels much brighter or much fainter than those covered by SCUBA surveys.

The predicted redshift distribution of sources brighter than 1 mJy at 850 μ m (Fig. 7) has a narrow peak at $z \sim 1$ mostly due to starburst galaxies, and a broad peak at $z \sim 2$ with an extended tail towards higher redshifts, due to star-forming spheroidal galaxies.

In Chapman et al. (2003), the spectroscopic redshifts of 10 representative SCUBA galaxies with $S_{850\mu m} > 5$ mJy have been reported. The median redshift of their sample is 2.4, with a

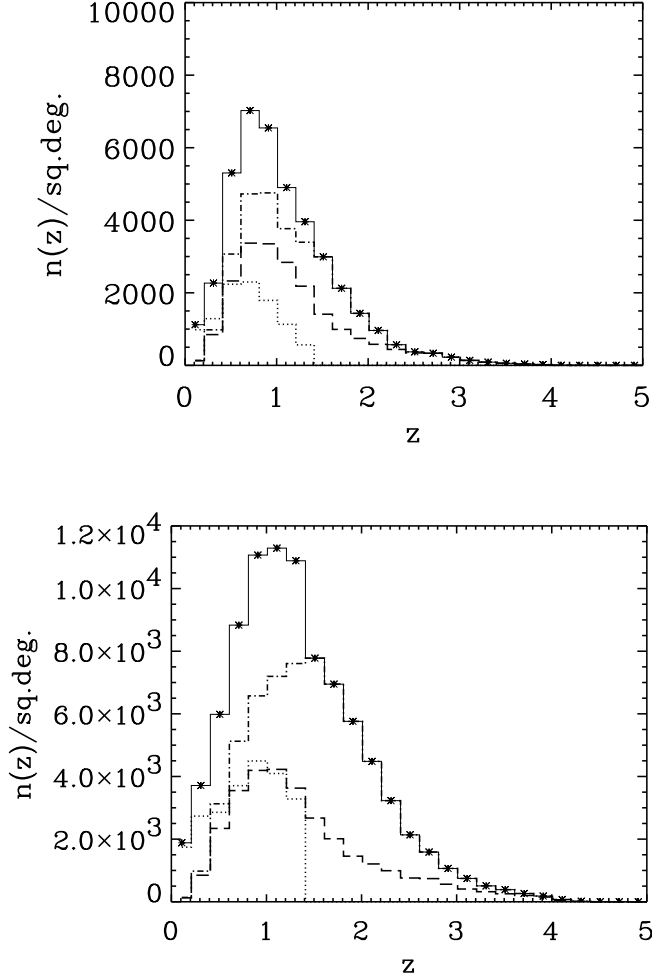


Fig. 19. Redshift distributions of sources with $S_{3.6\mu m} \geq 7.3 \mu\text{Jy}$ (upper panel) and $\geq 3 \mu\text{Jy}$, the SWIRE and GOODS limits respectively. Dot-dashed line: spheroids (the contribution of passively evolving spheroids is shown by the long-dashed line); dotted line: late type galaxies. The solid histogram with asterisks is the sum of all contributions. We expect to find $\approx 4 \times 10^4$ sources per square degree brighter than $7.3 \mu\text{Jy}$ and $\approx 9 \times 10^4$ sources per square degree brighter than $3 \mu\text{Jy}$. At both flux limits $\approx 73\%$ of the detected sources are spheroids. However, the proportion of those passively evolving decreases from $\approx 70\%$ at $7.3 \mu\text{Jy}$ to $\approx 50\%$ at $3 \mu\text{Jy}$.

quartile range of $z = 1.9 - 2.8$. The median and quartile range for our model are 2.48, 1.78 – 3.68 and 2.33, 1.78 – 3.15 respectively for the total (spheroids and late type galaxies) and spheroids alone, in remarkably good agreement.

While the sub-mm counts are informative on the star-formation phase of the evolution of spheroidal galaxies, the K-band counts in the range $14 \lesssim K \lesssim 19$ (Fig. 5) are dominated by the passive evolution phase. Fainter than $K \sim 19$ also star-forming spheroids begin to show-up and become increasingly important at fainter magnitudes. The brighter (in terms of apparent magnitude) such objects are those of lower bolometric

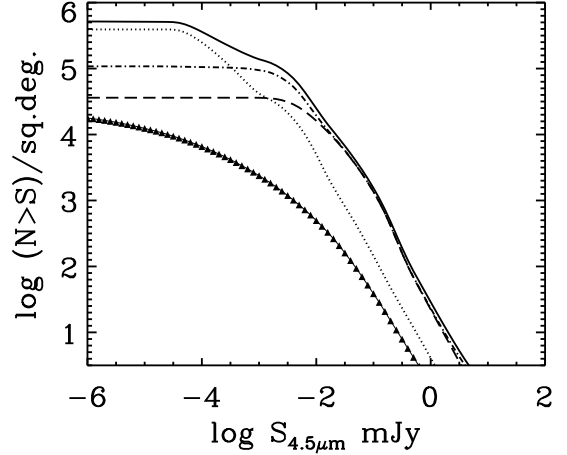


Fig. 20. Predicted $4.5\mu\text{m}$ IRAC source counts. The lines have the same meaning as in Fig. 18.

metric luminosity, which, in the GDS04 model, have a prolonged star-formation phase extending to $z \lesssim 1$ and whose stars are kept within a high optical depth environment for a time $t_e = 0.05$ Gyr (see Sect. 3). This is illustrated by Fig. 8, showing that, for $K \leq 20$, the contribution from star-forming spheroids peaks at z somewhat smaller than 1. Passively evolving spheroids essentially disappear at $K \geq 23$. The observed high- z tails of the distributions for $K \leq 23$ (Fig. 9) and for $K \leq 24$ (Fig. 10) are thus mostly due to star-forming spheroids. At these faint magnitudes, the K-band counts are dominated by late-type galaxies, which account for the big peak in the range $0.2 \leq z \leq 0.9$ (Figs. 9 and 10), as well as for the low- z shoulder at $K \leq 20$ (Fig. 8).

Note that the contribution of late type galaxies at faint flux limits may be underestimated. In fact the Subaru Deep Field source counts by Totani et al. (2001) (the triangles in Fig. 5) are raw data. Maihara et al. (2001) provide the counts corrected for incompleteness. However, as stated by the authors, the correction is model-dependent. A mild density evolution ($\sim (1+z)^{1.3}$) of dwarf galaxies would be sufficient to fit the corrected faint K-band counts. But the redshift distributions by Kashikawa et al. (2003) (Figs. 9 and 10) refer to actually observed sources, without any correction for incompleteness. We have thus chosen to adopt the simple assumption of no evolution for dwarves, which yields faint K-band counts consistent with the uncorrected data.

Passively evolving spheroids also dominate the $6.7\mu\text{m}$ ISOCAM counts (Altieri et al. 1999; Flores et al. 1999; Oliver et al. 2002; Sato et al. 2003; Metcalfe et al. 2003; Fig. 11) below $\sim 300 \mu\text{Jy}$, while at brighter flux densities late type galaxies take over. The model redshift distribution (lower panel of Fig. 11) is compatible with the (very limited) redshift information (Flores et al. 1999, Sato et al. 2004).

On the contrary, we interpret the observed IRAS $60\mu\text{m}$ and ISOPHOT $90\mu\text{m}$ counts (Figs. 12 and 13) as dominated by spiral and starburst galaxies, although star-forming spheroidal galaxies may start contributing to the deepest $90\mu\text{m}$ point.

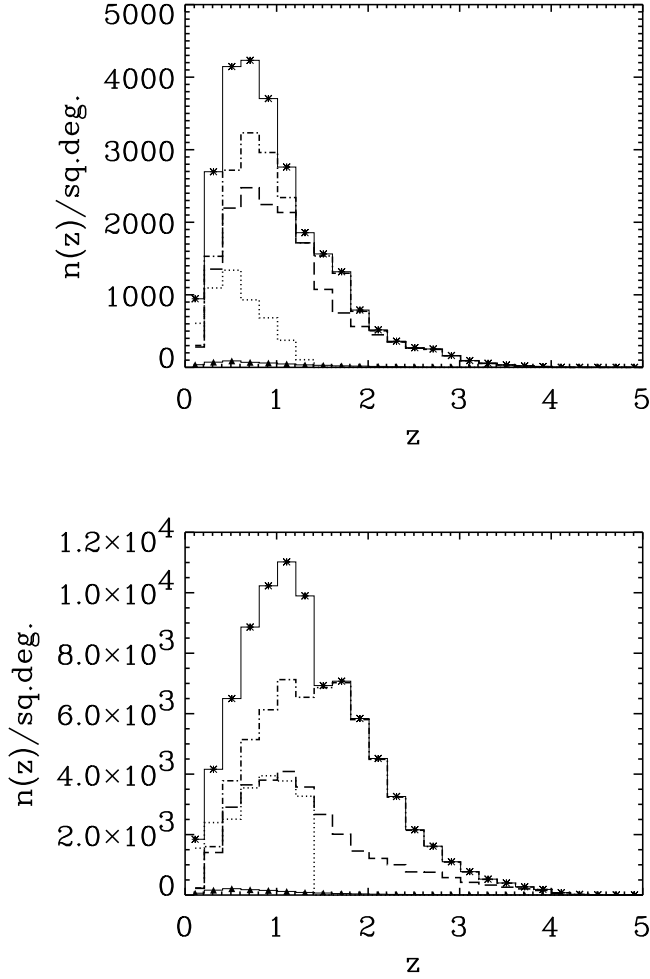


Fig. 21. Redshift distributions of sources with $S_{4.5\mu m} \geq 9.7 \mu\text{Jy}$ (upper panel) and $\geq 3 \mu\text{Jy}$, the SWIRE and GOODS limits respectively. Dot-dashed line: spheroids (the contribution of passively evolving spheroids is shown by the long-dashed line); dotted line: late type galaxies; filled triangles: AGNs. The solid histogram with asterisks is the sum of all contributions. We expect to find $\approx 2.5 \times 10^4$ sources per square degree brighter than $9.7 \mu\text{Jy}$, $\approx 80\%$ of which are spheroids (80% of which passively evolving) and $\approx 8.7 \times 10^4$ sources per square degree brighter than $3 \mu\text{Jy}$, $\approx 74\%$ of which are spheroids, almost equally subdivided among the star-forming and passive evolution phases.

Starburst galaxies dominate the $60 \mu\text{m}$ counts, except at the brightest fluxes, while their contribution to the ISOPHOT $90 \mu\text{m}$ counts is comparable to that of normal late-type galaxies. The predicted z -distribution at the latter wavelengths (lower panel of Fig. 13) compares favourably with the observational determination by Rowan-Robinson et al. (2003).

GRASIL yields the SED of galaxies all the way to radio frequencies, both for spheroids and for our templates for late-type galaxies (see Bressan, Silva & Granato 2002 for details). Furthermore, we have adopted the Dunlop & Peacock (1990) models to take into account radio galaxies. The predicted con-

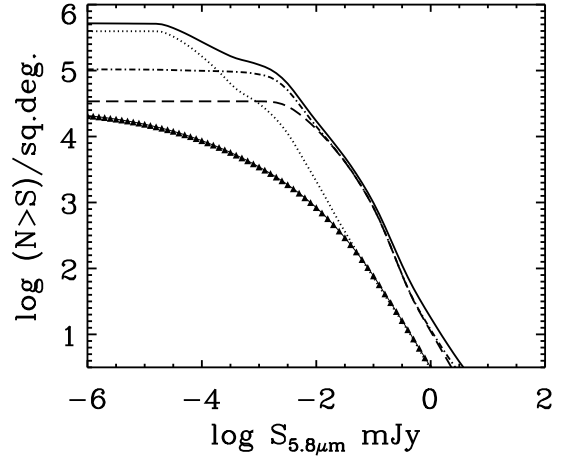


Fig. 22. Predicted $5.8 \mu\text{m}$ IRAC source counts. The lines have the same meaning as in Fig. 18.

tributions of the various populations to the 1.4 GHz counts are shown in Fig. 14. In the flux density range $1 \mu\text{Jy} \lesssim S_{1.4\text{GHz}} \lesssim 30 \mu\text{Jy}$ we expect that the counts are dominated by starburst and star-forming spheroidal galaxies, with comparable contributions.

4.2. Extremely Red Objects

Extremely red objects (EROs), with $R - K > 5$, have received special attention in recent years (Daddi et al. 2000; Smith et al. 2002; Roche et al. 2002, 2003; Cimatti et al. 2002, 2003; Takata et al. 2003; Yan & Thompson 2003; Yan et al. 2004; Webb et al. 2004; Moustakas et al. 2004), since their properties set crucial constraints on the early evolutionary phases of massive spheroidal galaxies. EROs are actually a mix of dusty star-forming and evolved galaxies formed at high redshifts (Cimatti et al. 2002, 2003; Mohan et al. 2002).

We have worked out the counts and the redshift distribution of both star-forming and passively evolving spheroidal galaxies brighter than $K = 19.2, 20, 20.3$ that, according to our model, have ERO colours. Note that the observed redshift distributions may be incomplete at high- z (Yan et al. 2004); also, a mild star formation activity, either due to residual gas or induced occasionally by interactions, neglected by our simple model, could decrease the number of galaxies with ERO colours, particularly at high redshifts. On the whole, the agreement with observations, which turn out to be very challenging for the other semi-analytic models (e.g., Somerville et al. 2004) is quite good (Fig. 15 and 16).

4.3. The IR background

One further important constraint on the models comes from the IR background. In Fig. 17 we compare the $1 - 1000 \mu\text{m}$ background spectrum yielded by our model with the data collected by Hauser & Dwek (2001). The dotted line shows the summed contributions of normal late-type and starburst galaxies. The

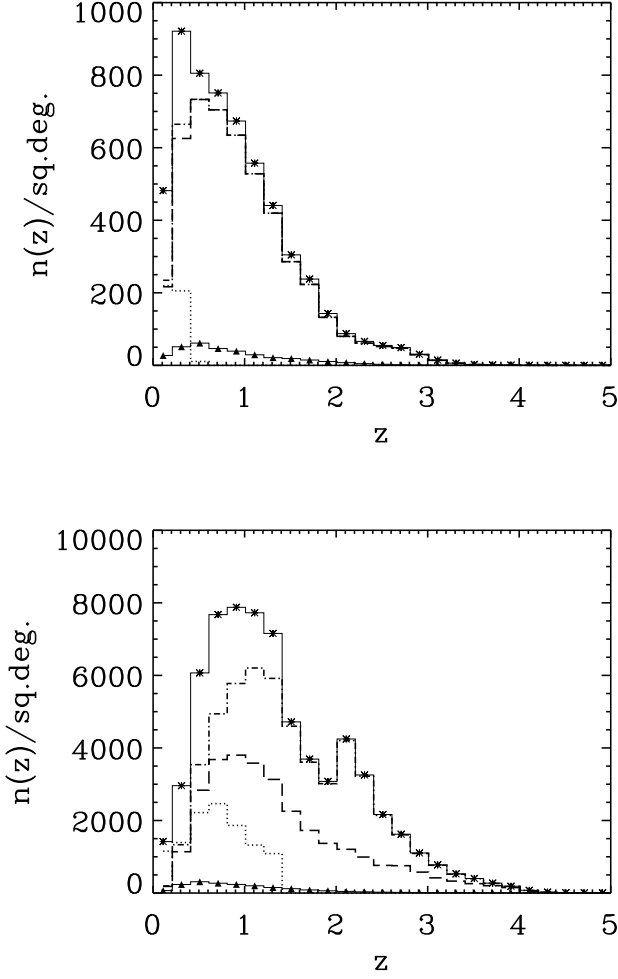


Fig. 23. Predicted redshift distributions of sources with $S_{5.8\mu\text{m}} \geq 27.5 \mu\text{Jy}$ (upper panel) and $\geq 3 \mu\text{Jy}$, the SWIRE and GOODS limits respectively. The lines have the same meaning as in Fig. 21. We expect $\approx 5.6 \times 10^3$ sources per square degree brighter than $27.5 \mu\text{Jy}$, $\approx 86\%$ of which are spheroids (all passively evolving) and $\approx 6.5 \times 10^4$ sources per square degree brighter than $3 \mu\text{Jy}$, $\approx 80\%$ of which are spheroids, \sim half of which are passively evolving.

leap at $10 \mu\text{m}$ corresponds to the transition between the evolutionary regime adopted in the MIR to mm region (Sect. 2.3.1) and the no-evolution one adopted in the NIR (Sect. 2.3.2). This sharp transition is clearly an over-simplification and results, in particular, in an underestimate of the contribution of late-type galaxies to the background intensity. The underestimate is likely to be quite large at wavelengths just below $10 \mu\text{m}$.

In the wavelength range $10 \mu\text{m} \leq \lambda \leq 150 \mu\text{m}$ the background is dominated by starburst galaxies, while at shorter wavelengths, spheroidal galaxies (mostly passively evolving) take over. Longward of $\lambda \approx 150 \mu\text{m}$ star-forming spheroids dominate if the starburst SED is similar to that of M82 (lower panel). In the case of a cooler starburst SED, like that of NGC6090 (upper panel), the contribution of starburst galaxies

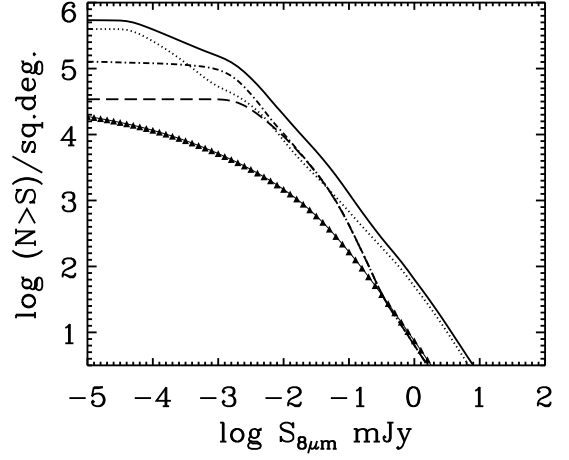


Fig. 24. Predicted $8 \mu\text{m}$ IRAC source counts. The lines have the same meaning as in Fig. 18.

to the sub-mm background may be comparable to that of star-forming spheroidal galaxies. The actual contribution of starburst galaxies is likely to be intermediate since, as noted above, they show a variety of SEDs, and their colours are correlated with luminosity.

5. Predictions for Spitzer Space Telescope surveys

We will focus on the two major extragalactic surveys carried out with the Spitzer Space Telescope (formerly SIRTf): the SIRTf Wide-area InfraRed Extragalactic survey (SWIRE; Lonsdale et al. 2003) and the Great Observatories Origins Deep Survey (GOODS; Dickinson et al. 2003). SWIRE will survey $60\text{--}65 \text{ deg}^2$ at high Galactic latitude in the four bands (3.6 , 4.5 , 5.6 , and $8 \mu\text{m}$) of the InfraRed Array Camera (IRAC) and in the three bands (24 , 70 , and $160 \mu\text{m}$) of the Multiband Imaging Photometer for SIRTf (MIPS). GOODS will provide deep images of approximately 300 arcmin^2 and ultra-deep images of two small fields in all IRAC bands, as well as deep exposures with MIPS at $24 \mu\text{m}$. The model counts and redshift distributions in each of the IRAC and MIPS bands are shown in Figs. 18 to 29.

The IRAC surveys will probe in depth the evolution of spheroidal galaxies. The surveys to the SWIRE sensitivity limits (7.3 , 9.7 , 27.5 , and $32.5 \mu\text{Jy}$ at 3.6 , 4.5 , 5.8 , and $8 \mu\text{m}$, respectively; Lonsdale et al. 2003) will primarily test the passive evolution phase, although star-forming spheroids will begin to peep out particularly at the shorter wavelengths. GOODS is expected to reach a limit of a $\sim 2\text{--}3 \mu\text{Jy}$ in all the IRAC bands. At this flux density limit, the majority of detected sources are expected to be spheroidal galaxies, about half of which in the active star-forming phase. Their redshift distribution at $3.6 \mu\text{m}$ will peak in the range $0.6\text{--}1$ or around $z \approx 1.5$ for the SWIRE and GOODS surveys, respectively. The peak due to star-forming spheroids moves, at the GOODS flux limit, to higher and higher redshifts with increasing wavelengths, up to

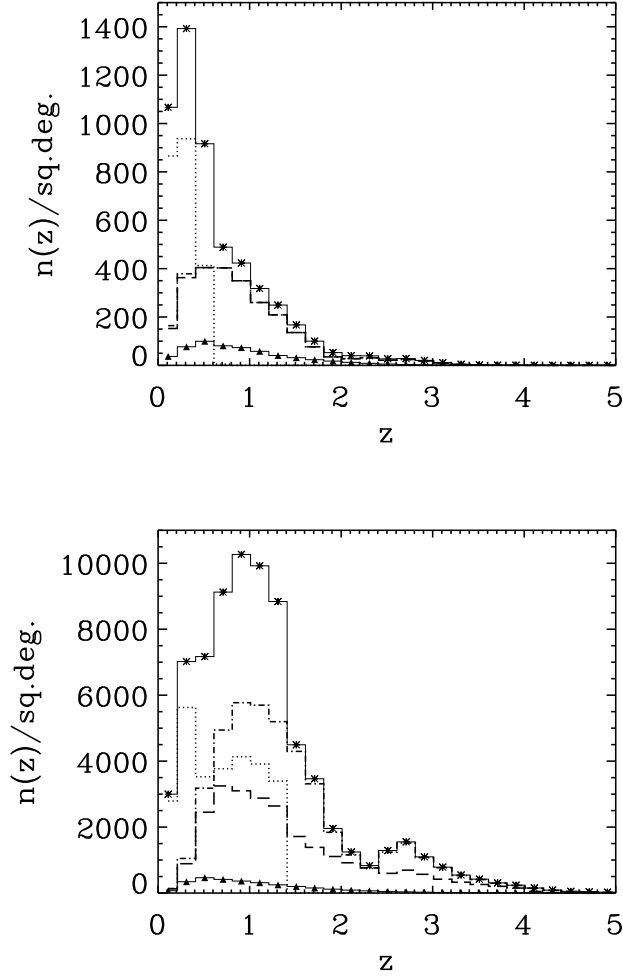


Fig. 25. Redshift distributions of sources with $S_{8\mu\text{m}} \geq 32.5 \mu\text{Jy}$ (upper panel) and $\geq 3 \mu\text{Jy}$, the SWIRE and GOODS limits respectively. The lines have the same meaning as in Fig. 21. We expect $\approx 5 \times 10^3$ sources per square degree brighter than $32.5 \mu\text{Jy}$, $\approx 50\%$ of which are spheroids (essentially all passively evolving) and $\approx 7.5 \times 10^4$ sources per square degree brighter than $3 \mu\text{Jy}$, $\approx 60\%$ of which are spheroids, the star-forming and passive evolution phases being almost equally represented.

$z \approx 2.7$ at $8 \mu\text{m}$. The peak of the overall distribution, for the GOODS survey, will keep at $z \approx 1$, due to the contribution of late-type galaxies. We caution that, as noted in Sect. 4.1, the contribution of late-type galaxies is likely to be underestimated at the shortest IRAC wavelengths because of our assumption of no-evolution at $\lambda < 10 \mu\text{m}$.

The GOODS survey in the $24 \mu\text{m}$ MIPS band is likely to be, because of the limited spatial resolution, confusion limited. Adopting Condon's (1974) approach to estimate the confusion noise, σ_{conf} , our model implies (neglecting the effect of clustering, discussed by Negrello et al. 2004, as well as the cirrus noise) a $5\sigma_{\text{conf}}$ detection limits, $S_{\text{lim,conf}}$, of 0.17 mJy , in good agreement with the earlier estimates summarized in Table 3 of Lonsdale et al. (2003). These estimates are well above the flux

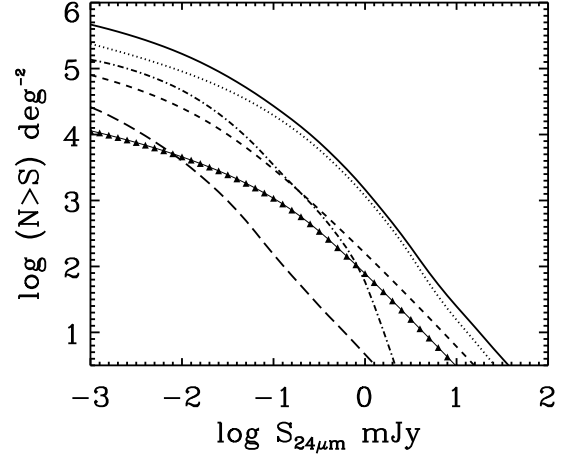


Fig. 26. Predicted contributions to the $24 \mu\text{m}$ Spitzer/MIPS source counts. Dot-dashed line: spheroids (all); long-dashed line: passively evolving spheroids; dotted line: starbursts; dashed line: spirals; filled triangles: AGNs.

limit aimed at by the GOODS survey ($20\text{--}80 \mu\text{Jy}$; Dickinson et al. 2003), but a factor of about 2.6 below the SWIRE sensitivity limit (0.45 mJy). We expect that both the SWIRE and the GOODS surveys at this wavelength are dominated by starburst galaxies, however with an 8–10% contribution from star-forming spheroids at redshifts in the range 1.5–3.

For the other MIPS bands we find $S_{\text{lim,conf}} = 10$ and 96 mJy at 70 and $160 \mu\text{m}$ respectively, in good agreement with Xu et al. (2003, model S3+E2) and well above the SWIRE sensitivities (2.75 and 17.5 mJy , respectively). Thus we expect SWIRE to be confusion limited at these wavelengths. The majority of sources detected to the estimated confusion limits should be starburst galaxies at $70 \mu\text{m}$, while star-forming spheroids may take over at $160 \mu\text{m}$. However, as discussed in Sect. 3, our model is likely to somewhat overestimate the counts at the latter wavelength.

6. Conclusions

Granato et al. (2001, 2004) have shown that the mutual feedback between star-forming spheroidal galaxies and the active nuclei growing in their cores can be a key ingredient towards overcoming one of the main challenges facing the hierarchical clustering scenario for galaxy formation, i.e. the fact that the densities of massive high redshift galaxies detected by SCUBA and by deep near-IR surveys are well above the predictions.

However, to take full advantage of the wealth of data on extragalactic sources that are rapidly accumulating in the IR to mm region to test evolutionary models and to assess their parameters, we need to deal with complex and poorly understood processes that determine the time-dependent SEDs of the various populations of galaxies. Indeed, semi-analytic models must rely on a large number of adjustable parameters. We have carried out a detailed comparison of the physically grounded GDS04 model, keeping their choice for the parameters control-

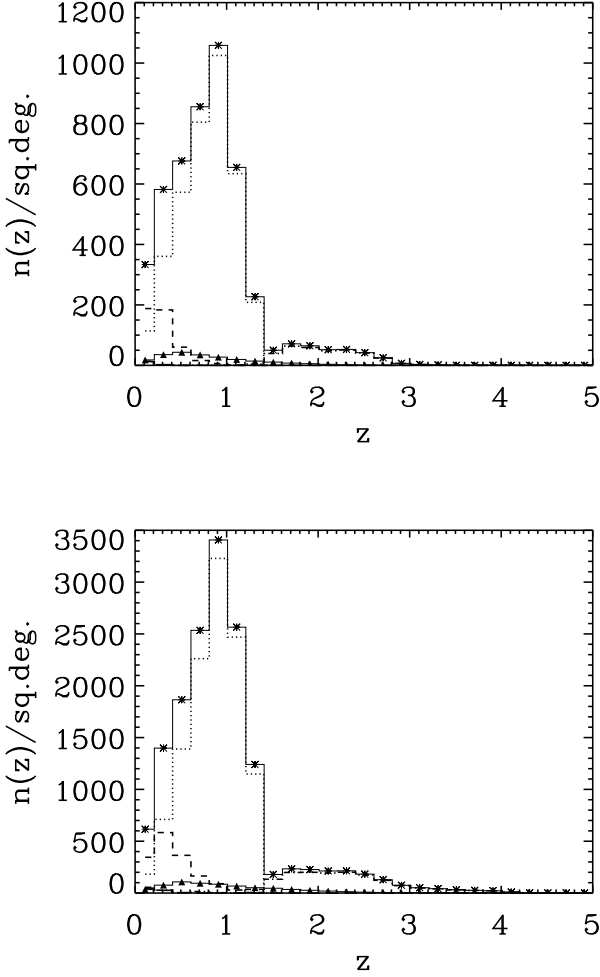


Fig. 27. Predicted redshift distributions for $S_{24\mu\text{m}} \geq 0.45$ mJy (the SWIRE flux density limit; upper panel) and $S_{24\mu\text{m}} \geq 0.17$ mJy (the estimated 5σ confusion limit). At these limits we will have, respectively, a total of $\sim 4.7 \times 10^3$ and $\sim 1.5 \times 10^4$ sources per square degree, 8 – 10% of which will be star forming spheroids. Dot-dashed line: spheroids; dotted line: starbursts; dashed line: spirals; filled triangles: AGNs.

ling the star-formation history, the chemical enrichment and the evolution of dust and gas content of massive spheroidal galaxies. We are therefore left with only two adjustable parameters, affecting their near-IR to mm SED (see Sect. 2.2) computed using the code GRASIL that includes a full treatment of starlight reprocessing by dust; as described in Sect. 3, their values are constrained mostly by $15\mu\text{m}$ and K -band counts. A simplified phenomenological approach (Sect. 2.3) has been adopted to deal with the other relevant galaxy populations (normal late-type and starburst galaxies), and the contribution by AGN has been estimated by coupling the cosmological evolution of AGN in the X-ray bands with detailed SEDs (Sect. 2.4).

The model predictions have then been tested against a broad variety of observational data, including, in addition to the $15\mu\text{m}$ and K -band counts, the redshift distributions of sources

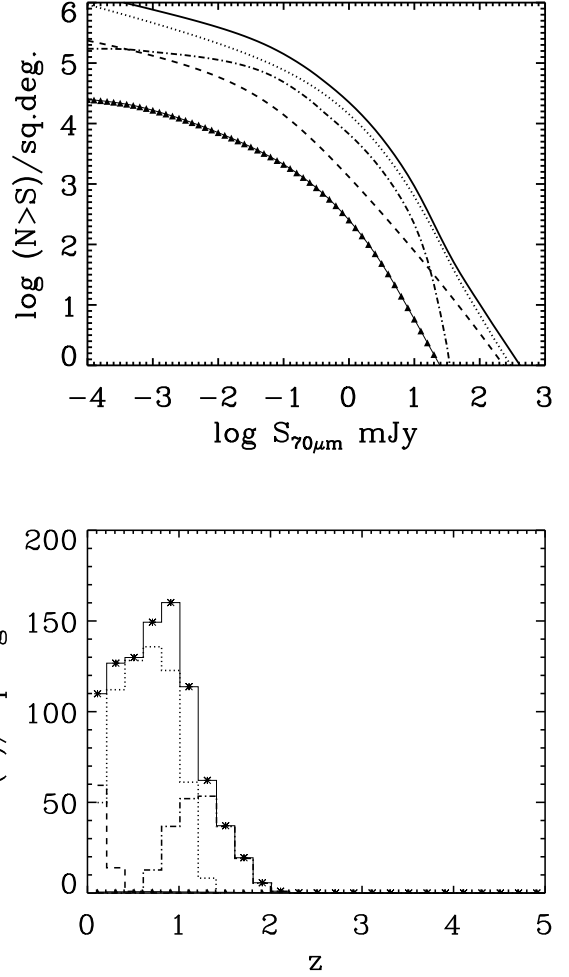


Fig. 28. Predicted $70\mu\text{m}$ source counts and redshift distribution for $S_{70\mu\text{m}} \geq 10$ mJy. Dot-dashed line: (star-forming) spheroids; dotted: starbursts; dashed: spirals; filled triangles: AGN. The thin solid histogram with asterisks in the lower panel shows the sum of all contributions. We expect ~ 900 sources per square degree brighter than 10 mJy; $\sim 23\%$ of them are spheroids.

brighter than 0.1 and 1 mJy at $15\mu\text{m}$, the SCUBA counts at $850\mu\text{m}$, the available (although still scanty) data on the redshift distribution of sources brighter than 5 mJy at $850\mu\text{m}$, the ISOPHOT 90 and $170\mu\text{m}$ counts and the corresponding redshift distributions, the IRAS $60\mu\text{m}$ counts, the radio 1.4 GHz counts, the ISOCAM $6.7\mu\text{m}$ counts and redshift distribution, the redshift distributions of galaxies to the magnitude limits $K = 20, 23$, and 24, and the $1\text{--}1000\mu\text{m}$ background spectrum. Specific predictions for the K -band counts and redshift distributions of EROs have been worked out and compared with data.

Encouraged by the good agreement of model predictions with all these data sets, we have worked out detailed predictions for the GOODS and SWIRE surveys with the Spitzer Space Telescope. In agreement with previous estimates, we find that the GOODS deep survey at $24\mu\text{m}$ and the SWIRE surveys at

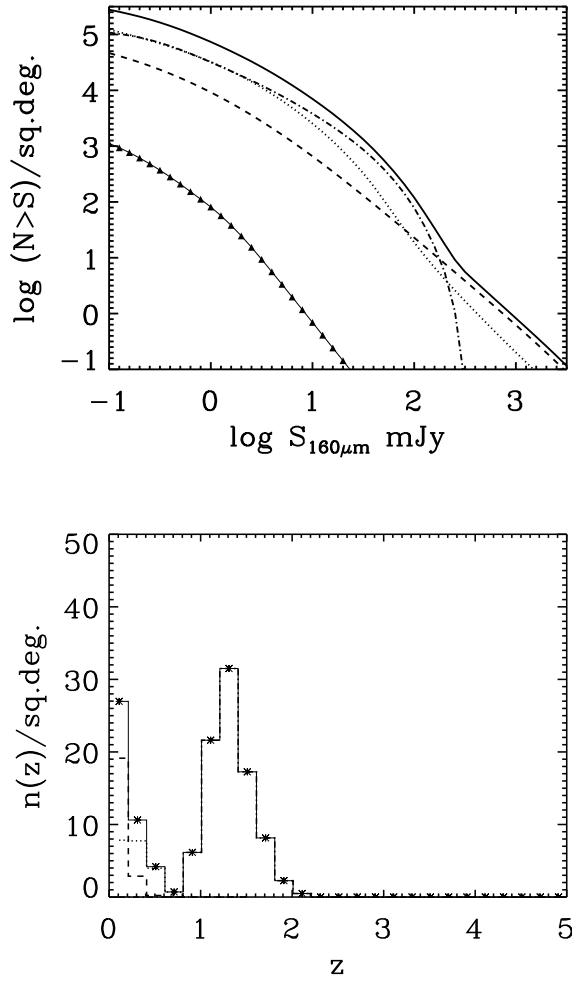


Fig. 29. Predicted $160\mu\text{m}$ source counts and redshift distribution for $S_{160\mu\text{m}} \geq 96 \text{ mJy}$, the expected 5σ confusion limit. Dot-dashed line: spheroids; dotted line: starbursts; dashed line: spirals; filled triangles: AGN. The thin solid histogram with asterisks in the lower panel is the sum of the various contributions. We expect ~ 130 sources per square degree brighter than 96 mJy ; $\sim 65\%$ of them are spheroids.

70 and $160\mu\text{m}$ are likely to be severely confusion limited. The GOODS surveys in the IRAC channels (3.6 to $8\mu\text{m}$), reaching flux limits of a few μJy , are expected to resolve most of the background at these wavelengths, to explore the full passive evolution phase of spheroidal galaxies and most of their active star-forming phase, detecting galaxies up to $z \approx 4$ and beyond. A substantial number of high z star-forming spheroidal galaxies should also be detected by the $24\mu\text{m}$ SWIRE and GOODS surveys, while the 70 and $160\mu\text{m}$ surveys will be particularly useful to study the evolution of such galaxies in the range $1 \lesssim z \lesssim 2$. However, starburst galaxies at $z \lesssim 1-1.5$ are expected to be the dominant population in MIPS channels, except, perhaps, at $160\mu\text{m}$.

We plan to apply our model to make predictions for the forthcoming surveys with Herschel, Planck, LMT and ALMA.

Acknowledgements. Work supported in part by MIUR (through a COFIN grant) and ASI. LS and GLG acknowledge kind hospitality by INAOE where part of this work was performed. We thank Andrea Cimatti for helpful discussions and for providing the redshifts of EROs in advance of publication. The LSGLG foundation is warmly acknowledged.

References

- Altieri, B., Metcalfe, L., Kneib, J.P., et al. 1999, *A&A*, 343, L65
Aussel, H., Cesarsky, C.J., Elbaz, D., & Starck, J.L. 1999, *A&A*, 342, 313
Barger, A. J., Cowie, L. L., Sanders, D. B. 1999, *ApJL*, 518, 5
Benson, A.J., Bower, R.G., Frenk, C.S., Lacey, C.G., Baugh, C.M., & Cole, S. 2003, *ApJ*, 599, 38
Bertin, E., Dennefeld, M., & Moshir, M. 1997, *A&A*, 323, 685
Binney, J. 2004, *MNRAS*, 347, 1093
Blain, A. W., Kneib, J.-P., Ivison, R. J., Smail, I. 1999, *ApJ*, 512, 87
Borys, C., Chapman, S. C., Halpern, M., Scott, D. 2002, *MNRAS*, 330, 63
Bressan, A., Silva, L., & Granato, G. L. 2002, *A&A*, 392, 377
Caputi, K.I., Dunlop, J.S., McLure, R.J., & Roche, N.D. 2004, *MNRAS*, submitted (astro-ph/0401047)
Chapman, S.C., Blain, A.W., Ivison, R.J., & Smail, I.R. 2003, *Nat*, 422, 695
Chapman, S.C., Helou, G., Lewis, G.F., & Dale, D.A. 2003, *ApJ*, 588, 186
Chapman, S.C., Smail, I., Ivison, R.J., Helou, G., Dale, D.A., & Lagache, G. 2002, *ApJ*, 573, 66
Ciliegi, P., McMahon, R. G., Miley, G., et al. 1999, *MNRAS*, 302, 222
Cimatti, A. 2003, *Ap&SS*, 285, 231
Cimatti, A., Daddi, E., Mignoli, M., et al. 2002, *A&A*, 381, L68
Cimatti, A., Daddi, E., Cassata, P., et al., 2003, *A&A*, 412, L1
Cole, S., Aragon-Salamanca, A., Frenk, C.S., Navarro, J.F., & Zepf, S.E. 1994, *MNRAS*, 271, 781
Cole, S., Lacey, C.G., Baugh, C.M., & Frenk, C.S. 2000, *MNRAS*, 319, 168
Condon, J.J. 1974, *ApJ*, 188, 279
Daddi, E., Cimatti, A., Pozzetti, L., Hoekstra, H., Rttgering, H. J. A., Renzini, A., Zamorani, G., & Mannucci, F. 2000, *A&A*, 361, 535
Daddi, E., Cimatti, A., Renzini, A., et al. 2004, *ApJ*, 600, L127
Dale, D.A., Silbermann, N.A., Helou, G., et al., 2000, *AJ*, 120, 583
Dickinson, M., Giavalisco, M., the GOODS Team 2003, in prec. ESO Workshop “The Mass of Galaxies at Low and High Redshift”, R. Bender and A. Renzini eds., Springer-Verlag, p. 324
de Lapparent, V., Galaz, G., Bardelli, S., & Arnouts S. 2003, *A&A*, 404, 831
Dole, H., Gispert, R., Lagache, G., et al. 2001, *A&A*, 372, 702
Dunlop, J.S., & Peacock, J.A. 1990, *MNRAS*, 247, 19
Dwek, E. 1998, *ApJ*, 501, 643
Eales, S., Lilly, S., Webb, T., Dunne, L., Gear, W., Clements, D., Yun, M. 2000, *AJ*, 120, 2244
Efsthathiou, A., Oliver, S., Rowan-Robinson, M., et al. 2000, *MNRAS*, 319, 1169
Elbaz, D., Cesarsky, C. J., Fadda, D., et al. 1999, *A&A*, 351, 37
Elbaz, D., Cesarsky, C.J., Chanial, P., et al. 2002, *A&A*, 384, 848
Fadda, D., Flores, H., Hasinger, G., et al. 2002, *A&A*, 383, 838
Flores, H., Hammer, F., Dsert, F.X., et al. 1999, *A&A*, 343, 389
Franceschini, A., Aussel, H., Cesarsky, C.J., Elbaz, D., & Fadda D. 2001, *A&A*, 378, 1
Franceschini, A., Berta, S., Rigopoulou, D., et al. 2003, *A&A*, 403, 501

- Granato, G.L., Franceschini, A., & Danese, L. 1996, in “Unveiling the Cosmic Infrared Background”, ed. E. Dwek, AIP conf. proc. 348, 226
- Granato, G.L., Lacey, C.G., Silva, L., Bressan, A., Baugh, C.M., Cole, S., & Frenk, C.S. 2000, *ApJ*, 542, 710
- Granato, G.L., Silva, L., Monaco, P., Panuzzo, P., Salucci, P., De Zotti, G., & Danese L. 2001, *MNRAS*, 324, 757
- Granato, G.L., De Zotti, G., Silva, L., Bressan, A., & Danese, L. 2004, *ApJ*, 600, 580 (GDS04)
- Gruppioni, C., Zamorani, G., de Ruiter, H. R., Parma, P., Mignoli, M., & Lari, C. 1997, *MNRAS*, 286, 470
- Gruppioni, C., Ciliegi, P., Rowan-Robinson, M., et al. 1999, *MNRAS*, 305, 297
- Gruppioni, C., Lari, C., Pozzi, F., et al. 2002, *MNRAS*, 335, 831
- Hauser, M.G., & Dwek, E. 2001, *ARA&A*, 39, 249
- Hopkins, A., Afonso, J., Cram, L., & Mobasher, B. 1999, *ApJL*, 519, 59
- Hughes, D. H., Serjeant, S., Dunlop, J., et al. 1998, *Nature*, 394, 241
- Kashikawa, N., Takata, T., Ohya, Y., et al. 2003, *AJ*, 125, 53
- Kauffmann, G., Colberg, J.M., Diaferio, A., & White, S.D.M., 1999, *MNRAS*, 303, 188
- Kauffmann, G., White, S.D.M., & Guiderdoni, B. 1993, *MNRAS*, 264, 201
- Kaviani, A., Haehnelt, M.G., & Kauffmann, G. 2003, *MNRAS*, 340, 739
- Kochanek, C. S., Pahre, M. A., Falco, E. E., et al. 2001, *ApJ*, 560, 566
- Lacey, C., Guiderdoni, B., Rocca-Volmerange, B., & Silk, J. 1993, *ApJ*, 402, 15
- Lagache, G., Dole, H., Puget, J.-L. 2003, *MNRAS*, 338, 555
- Lonsdale, C. J., Hacking, P. B., Conrow, T. P., Rowan-Robinson, M. 1990, *ApJ*, 358, 60
- Lonsdale, C.J., Smith, H.E., Rowan-Robinson, M. et al., 2003, *PASP*, 115, 897
- Maihara, T., Iwamuro, F., Tanabe, H., et al. 2001, *PASJ*, 53, 25
- Mannucci, F., Pozzetti, L., Thompson, D., Oliva, E., Baffa, C., Comoretto, G., Gennari, S., & Lisi, F. 2002, *MNRAS*, 329, L57
- Mazzei, P., Aussel, H., Xu, C., Salvo, M., De Zotti, G., & Franceschini, A. 2001, *NewA*, 6, 265
- Metcalfe, L., Kneib, J.-P., McBreen, B., et al. 2003, *A&A*, 407, 791
- Mohan, N.R., Cimatti, A., Röttgering, H.J.A., Andreani, P., Severgnini, P., Tilanus, R.P.J., Carilli, C.L., & Stanford, S.A. 2002, *A&A*, 383, 440
- Moustakas, L. A., Davis, M., Graham, J. R., Silk, J., Peterson, B. A., Yoshii, Y. 1997, *ApJ*, 475, 445
- Moustakas, L.A., Casertano, S., Conselice, C., et al. 2004, *ApJ*, 600, L131
- Miyazaki, M., Shimasaku, K., Kodama, T., et al. 2003, *PASJ*, 55, 1079
- Negrello, M., Magliocchetti, M., Moscardini, L., De Zotti, G., Granato, G.L., & Silva L. 2004, *MNRAS*, submitted (astro-ph/0401199)
- Oliver, S., Goldschmidt, P., Franceschini, A., et al. 1997, *MNRAS*, 289, 471
- Oliver, S., Mann, R.G., Carballo, R., et al. 2002, *MNRAS*, 332, 536
- Patris, J., Dennefeld, M., Lagache, G., & Dole, H. 2003, *A&A*, 412, 349
- Pearson, C., & Rowan-Robinson, M. 1996, *MNRAS*, 283, 174
- Poli, F., Giallongo, E., Fontana, A., et al. 2003, *ApJ*, 593, L1
- Pozzetti, L., Cimatti, A., Zamorani, G., et al., 2003, *A&A*, 402, 837
- Pozzi, F., Ciliegi, P., Gruppioni, C., et al. 2003, *MNRAS*, 343, 1348
- Richards, E. A. 2000, *ApJ*, 533, 611
- Roche, N.D., Almaini, O., Dunlop, J., Ivison, R.J., & Willott, C.J. 2002, *MNRAS*, 337, 1282
- Roche, N.D., Dunlop, J., & Almaini, O. 2003, *MNRAS*, 346, 803
- Rodighiero, G., Lari, C., Franceschini, A., Gregnanin, A., Fadda, D. 2003, *MNRAS*, 343, 1155
- Romano, D., Silva, L., Matteucci, F., & Danese, L. 2002, *MNRAS*, 334, 444
- Rowan-Robinson, M., Lari, C., Perez-Fournon, I., et al. 2003, *astro-ph/0308283*
- Sajina, A., Borys, C., Chapman, S., Dole, H., Halpern, M., Lagache, G., Puget, J.-L., & Scott, D. 2003, *MNRAS*, 343, 1365
- Saracco, P., Giallongo, E., Cristiani, S., et al. 2001, *A&A*, 375, 1
- Sato, Y., Kawara, K., Cowie, L.L., et al. 2003, *A&A*, 405, 833
- Sato, Y., Cowie, L.L., Kawara, K., et al. 2004, *AJ*, in press (astro-ph/0312114)
- Saunders, W., Rowan-Robinson, M., Lawrence, A., Efstathiou, G., Kaiser, N., Ellis, R.S., & Frenk, C.S. 1990, *MNRAS*, 242, 318
- Serjeant, S., Oliver, S., Rowan-Robinson, M., et al. 2000, *MNRAS*, 316, 768
- Severgnini, P., Maiolino, R., Brusa, M., Cimatti, A., Comastri, A., Fiore, F., & Vignali C. 2003, *RMxAC*, 17, 270
- Silva, L. 1999, Ph.D. thesis, SISSA, Trieste
- Silva, L., Granato, G.L., Bressan, A., & Danese, L. 1998, *ApJ*, 509, 103
- Silva, L., Maiolino, R., & Granato, G. L. 2004, in preparation
- Smith, G.P., Smail, I., Kneib, J.-P., et al. 2002, *MNRAS*, 330, 1
- Somerville, R.S., Moustakas, L.A., Mobasher, B., et al. 2004, *ApJ*, 600, L135
- Somerville, R.S., & Primack, J.R. 1999, *MNRAS*, 310, 1087
- Stickel, M., Lemke, D., Klaas, U., et al. 2000, *A&A*, 359, 865
- Takata, T., Kashikawa, N., Nakanishi, K., et al. 2003, *PASJ*, 55, 789
- Taniguchi, Y., Cowie, L. L., Sato, Y., et al. 1997, *A&A*, 328, 9
- Thomas, D. 1999, *MNRAS*, 306, 655
- Thomas, D., Maraston, C., & Bender, R. 2002, *Ap&SS*, 281, 371
- Totani, T., Yoshii, Y., Maihara, T., Iwamuro, F., Motohara, K. 2001, *ApJ*, 559, 592
- Ueda, Y., Akiyama, M., Ohta, K., & Miyaji, T. 2003, *ApJ*, 598, 886
- Webb, T., Brodwin, M., Eales, S., & Lilly, S. 2004, *ApJ*, in press (astro-ph/0311598)
- Windhorst, R. A., Fomalont, E. B., Partridge, R. B., & Lowenthal, J. D. 1993, *ApJ*, 405, 498
- Xu, C., Lonsdale, C.J., Shupe, D.L., O’Linger, J., & Masci, F. 2001, *ApJ*, 562, 179
- Xu, C.K., Lonsdale, C.J., Shupe, D.L., Franceschini, A., Martin, C., & Schiminovich, D. 2003, *ApJ*, 587, 90
- Yan, L., & Thompson, D. 2003, *ApJ*, 586, 765
- Yan, L., Thompson, D., & Soifer, T. 2004, *AJ*, in press (astro-ph/0312142)